Evaluating a Positive Allosteric Modulator Radiotracer Candidate to Image the Dopamine D1 Receptor

Megan Verma

Thesis submitted to the Faculty of Medicine in partial fulfillment of the requirements for the Master of Science in Biochemistry

Department of Biochemistry, Microbiology and Immunology
Faculty of Medicine
University of Ottawa

ABSTRACT

The dopamine D1 receptor (D1R) is the most populous dopaminergic G-protein coupled receptor, triggering functional responses associated with cognition and movement. Although receptor abnormalities correlate with prevalent neurological conditions like Parkinson's disease and schizophrenia, the relationship between D1R distribution and systemic dopaminergic outcomes requires further elucidation.

D1R antagonists have been radiolabelled for PET imaging, but they show suboptimal target selectivity. However, positive allosteric modulators (PAMs) display non-orthosteric binding, theoretically reducing off-target signals. Among such compounds, ASP4345 was examined in preliminary clinical trials and showed activity at rodent and human receptors. Thus, we aim to evaluate ASP4345 as a positive allosteric modulator D1R radiotracer candidate.

We synthesized ASP4345 over five steps and assessed molecular identity via NMR and mass spectrometry, achieving an overall yield of 86% in the final coupling step. Functional allostery was analyzed using dopamine and MLS1082, a known D1R PAM, in cAMP accumulation assays. In tandem, these experiments explored target selectivity by expressing the homologous dopamine D5 receptor (D5R). Subsequent analyses implied that ASP4345 binds to both D1-class receptors and exhibits a combined agonist-PAM profile.

Our next steps include identifying a radiolabeling precursor and analyzing *in vivo* binding in rodents through radiosynthetic screening and biodistribution experiments, respectively. Overall, these approaches will develop a PAM radiotracer workflow to study the dopaminergic system and eventually neurological disease.

ACKNOWLEDGEMENTS

I would like to begin by sharing my gratitude for the tireless support, guidance, and flexibility of my supervisor, Dr. Benjamin Rotstein. Throughout my time at the Molecular Imaging Probes and Radiochemistry Laboratory, Dr. Rotstein has always cultivated my curiosity and encouraged my diverse interests. His unwavering commitment to student success has built my confidence in research, so I hope to continue asking more questions than I can answer.

I also extend my thanks to Drs. Lauri Tuominen, Geneviève Laroche, Patrick Giguère, and Mario Tiberi for sharing their expertise on various aspects of this project. From learning about the clinical implications of dopaminergic imaging to GPCR modulation, I greatly valued our collaborators' insights and engagement. Furthermore, I appreciate the assistance of Anthony Carter for imparting his technical skills related to future animal work.

I want to highlight that my lab members have been an integral part of my journey. Whether we were sharing cafeteria pizza or hiding rubber ducks, I enjoyed all the fun we created between the science. And finally, to my dearest parents, sister, partner, and friends – thank you for anchoring me.

EPIGRAPH

But as if a magic lantern threw the nerves in patterns on a screen.

- T.S. Eliot

TABLE OF CONTENTS

ABSTRACT ..... **ii**

ACKNOWLEDGEMENTS ..... **iii**

EPIGRAPH ..... **iv**

LIST OF ABBREVIATIONS ..... **vii**

LIST OF FIGURES ..... **ix**

CHAPTER I: INTRODUCTION **1**

1.1. Overview of the Dopaminergic System 1

1.2. Dopamine Synthesis and Release 3

1.3. Dopamine Receptors 5

1.4. The Dopamine D1 Receptor 7

1.5. Clinical Relevance 7

1.5.1. Schizophrenia 8

1.5.2. Parkinson's Disease 8

1.6. Positron Emission Tomography and the Dopamine D1 Receptor 9

1.6.1. [^{11}C]SCH23390 12

1.6.2. [^{11}C]NNC112 13

1.6.3. Selectivity Issues 13

1.7. D1R-Ligand Interactions 14

1.7.1. Allosteric Modulation 14

1.8. D1R Positive Allosteric Modulator ASP4345 15

1.9. Hypothesis and Objectives 17

CHAPTER II: MATERIALS AND METHODS **18**

2.1. Materials 18

2.2. ASP4345 Standard Synthesis: 2-(5-chloro-2-oxo-1,3-benzoxazol-3(2*H*)-yl)-*N*-{[5-(trifluoromethyl)-1*H*-benzimidazol-2-yl]methyl} acetamide hydrochloride 18

2.2.1. Synthesis of (5-chloro-2-oxo-1,3-benzoxazol-3(2*H*)-yl) acetic acid 18

2.2.2. Synthesis of *N*-methyl-1-[5-(trifluoromethyl)-1*H*-benzimidazol-2-yl] methanamine dihydrochloride 19

2.2.3. Coupling of (5-chloro-2-oxo-1,3-benzoxazol-3(2*H*)-yl) acetic acid and *N*-methyl-1-[5-(trifluoromethyl)-1*H*-benzimidazol-2-yl] methanamine dihydrochloride 20

2.3. GloSensor Assays 23
2.4. Radiolabelling Strategy Screening 23
2.4.1. [^{11}C]CO_2 Fixation Aminophenol Precursor 23
2.4.2. Cu-mediated ^{18}F-Fluorination 29
2.4.3. Synthesis of ^{11}C-Methylation Acetamide Model Substrates 29
CHAPTER III: RESULTS 31
3.1. Synthesis of ASP4345 31
3.2. *In vitro* Pharmacological Characterization with GloSensor 31
3.2.1. Functional Allostery and Dose-Response Profile 33
3.3. Radiolabelling Strategy Screening 39
3.3.1. [^{11}C]CO_2 Fixation Aminophenol Precursor Routes 39
3.3.2. Cu-mediated ^{18}F-Fluorination 44
3.3.3. ^{11}C-Methylation Acetamide Model Substrates 46
CHAPTER IV: DISCUSSION 49
4.1. *In vitro* Pharmacological Characterization 49
4.2. Radiolabelling Strategy Screening 50
4.2.1. [^{11}C]CO_2 Fixation Aminophenol Precursor Routes 50
4.2.2. Cu-mediated ^{18}F-Fluorination 52
4.2.3. ^{11}C-Methylation 54
CHAPTER V: CONCLUSION 55
5.1. Summary 55
5.2. Future Directions 56
5.3. Closing Remarks 57
REFERENCES 58
APPENDIX 67
NMR Characterization Data 67
UPLC-MS Characterization Data 75
^{18}F-Fluorination Radio-TLC Data 80

LIST OF ABBREVIATIONS

AC – adenylate cyclase

ASP4345 – (2-(5-chloro-2-oxo-1,3-benzoxazol-3(2*H*)-yl)-*N*-{[5-(trifluoromethyl)-1*H*-benzimidazol-2-yl]methyl} acetamide hydrochloride)

^{11}C – carbon-11

cAMP – cyclic adenosine monophosphate

$CDCl_3$ – deuterated chloroform

CO_2 – carbon dioxide

D1R – dopamine D1 receptor

D2R – dopamine D2 receptor

D3R – dopamine D3 receptor

D4R – dopamine D4 receptor

D5R – dopamine D5 receptor

DMEM – Dulbecco's Modified Eagle Medium

DMF – dimethylformamide

DMSO – dimethyl sulfoxide

^{18}F – fluorine 18

FBS – fetal bovine serum

FLIPR - fluorescence imaging plate reader

GIRK - G-protein-coupled inwardly rectifying potassium channel

GPCR – G-protein coupled receptor

HBSS – Hanks' balanced salt solution

HCl – hydrochloric acid

HEK – human embryonic kidney

HEPES – 2-[4-(2-hydroxyethyl)piperazin-1-yl]ethanesulfonic acid

K_{222} – Kryptofix 222

K_2CO_3 – potassium carbonate

LC-MS/MS – liquid chromatography-mass spectrometry

L-DOPA – levodopa

MLS1082 – 2-cyclohexyl-10-methyl-3-phenylpyrimido[4,5]quinoline-4,5-dione

MEM – methoxyethoxy methyl ether

MPTP – 1-methyl-4-phenyl-1,2,3,6-tetrahydropyridine

MRM – multiple reaction monitoring

NMR – nuclear magnetic resonance

NNC112 – ((5*S*)-5-(1-benzofuran-7-yl)-8-chloro-3-methyl-1,2,4,5-tetrahydro-3-benzazepin-7-ol)

PAM – positive allosteric modulator

PD – Parkinson's disease

PET – positron emission tomography

PFC – prefrontal cortex

RCY – radiochemical yield

SCH23390 – ((5*R*)-8-chloro-3-methyl-5-phenyl-2,3,4,5-tetrahydro-1*H*-3-benzazepin-7-ol)

SCZ – schizophrenia

SN – substantia nigra

SND – striatonigral degeneration

TLC – thin-layer chromatography

UPLC-MS – ultra-performance liquid chromatography-mass spectrometry

VMAT2 – vesicular monoamine transporter 2

LIST OF FIGURES

Figure 1.1. - Dopaminergic Innervation of the Brain

Figure 1.2. - Synthesis and Release of Dopamine

Figure 1.3. - Overview of Dopaminergic Receptor Signalling Pathways

Figure 1.4. - Summary of Positron Emission Tomography

Figure 1.5. - Dopamine D1 Receptor Ligands

Figure 2.1. - Synthesis of ASP4345

Figure 3.1. - Illustration of the GloSensor Assay

Figure 3.2. - Evaluation of ASP4345 as a Positive Allosteric Modulator

Figure 3.3. - Characterization of ASP4345 Agonist Activity

Figure 3.4. - Analysis of ASP4345 Dose-Response Profile

Figure 3.5. - Assessment of ASP4345 Activity at D5R

Figure 3.6. - Proposed [^{11}C]CO_2 Fixation Radiolabelling Strategy

Figure 3.7. - Phenol Protection Options for [^{11}C]CO_2 Fixation Precursor

Figure 3.8. - Cu-mediated ^{18}F-Fluorination Derisking Experiment

Figure 3.9. - Adapting Radiosynthesis of [^{11}C]FMZ to ASP4345

Figure 3.10. - Synthesis of Acetamide Model Compounds for ^{11}C-Methylation

CHAPTER I: INTRODUCTION

1.1. Overview of the Dopaminergic System

The dopaminergic system is implicated in a vast array of behavioural and cognitive functions, ranging from rewards-based learning to movement.[1–3] To do so, dopamine stimulates postsynaptic receptors to transduce an effector response. This process is actualized between dopaminergic neurons which innervate the human brain along two major pathways: mesocorticolimbic and nigrostriatal (Figure 1.1).[1] The mesocorticolimbic circuit originates in the ventral tegmental area (VTA) and projects to the frontal cortex and nucleus accumbens.[4] Correspondingly, the nigrostriatal pathway begins in the midbrain substantia nigra (SN) and reaches the caudate putamen. Each neural network fulfills a distinct functional role, with the mesocorticolimbic and nigrostriatal pathways responsible for working memory and locomotor control, respectively.[1] As such, dopaminergic dysfunction in these circuits is linked to neurological disease. Aberrant mesocorticolimbic signalling is associated with memory-related cognitive deficits in schizophrenia, whereas nigrostriatal neuronal death correlates with motor impairment in Parkinson's disease.[5,6] Given this realm of clinical significance, the dopaminergic system presents a worthwhile investigative avenue.

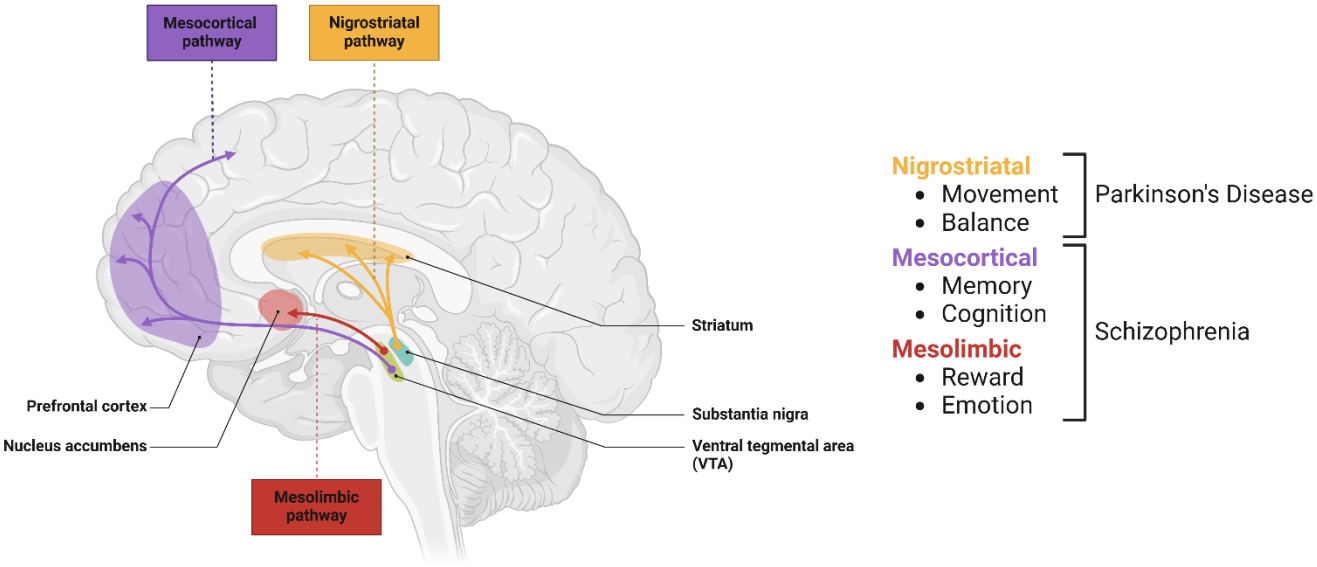

Figure 1.1. Dopaminergic Innervation of the Brain. The dopaminergic system is primarily comprised of the nigrostriatal and mesocorticolimbic pathways. These neural networks project from the substantia nigra and ventral tegmental area to the striatum, prefrontal cortex, and nucleus accumbens. Adapted from BioRender.

1.2. Dopamine Synthesis and Release

Dopamine is a monoaminergic neurotransmitter comprised of a catechol core and aminated side chain.[1,2] Its synthesis begins with the transfer of tyrosine across the blood-brain barrier by sodium-independent transport mechanisms for large neutral amino acids.[7–9] Upon entering the brain, tyrosine undergoes hydroxylation by tyrosine hydroxylase to produce the dopamine precursor, levodopa (L-DOPA) within dopaminergic neurons in the VTA and SN (Figure 1.2).[9] This molecule is then decarboxylated by aromatic l-amino acid decarboxylase, yielding dopamine. Next, the newly synthesized neurotransmitter is packaged into synaptic vesicles by vesicular monoamine transporter 2 (VMAT2).[1] Signalling events are initiated by presynaptic depolarization, whereupon the vesicles fuse with the plasma membrane to release dopamine into the interstitial fluid.[9] Neurotransmitters then bind to dopamine receptors on the receiving cell, triggering intracellular signalling cascades. To conclude the event, the dopamine transporter (DAT) ends transduction by transporting dopamine into the presynaptic neuron for vesicular reuptake by VMAT2 or monoamine oxidase-mediated catabolism.[1]

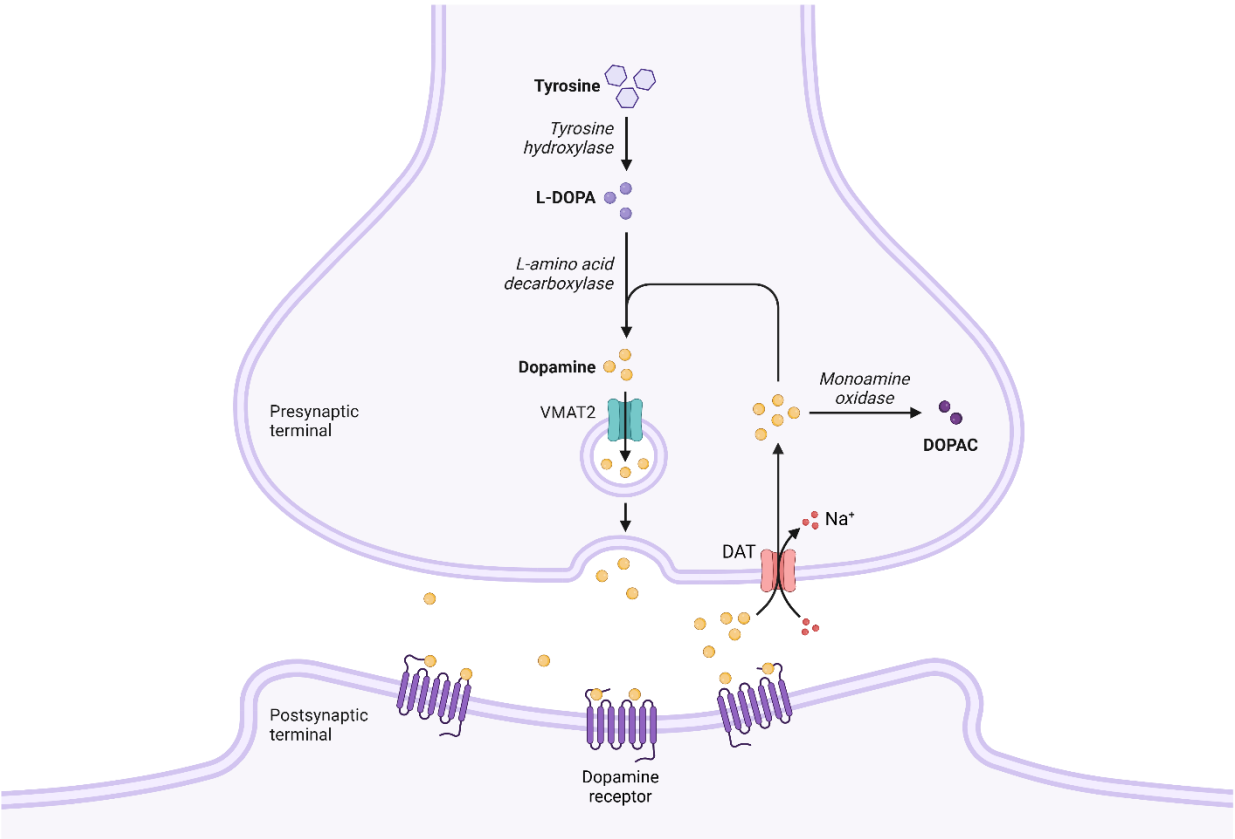

Figure 1.2. Synthesis and Release of Dopamine. The neurotransmitter dopamine is synthesized, packaged, and released from dopaminergic neurons in the substantia nigra and ventral tegmental area. Signalling events are enabled by dopamine receptors, after which DAT facilitates reuptake for vesicular repackaging or catabolism by monoamine oxidase. Adapted from BioRender.

1.3. Dopamine Receptors

Dopamine receptors are G-coupled protein receptors (GPCRs) structured across seven transmembrane domains, three extracellular loops, and three intracellular loops.[1,10] Dopaminergic GPCRs are classified as D1- or D2-like based on whether they stimulate or inhibit adenylate cyclase (AC), respectively. Biochemically, this is determined by the family of trimeric G-proteins with which they associate; D1-class receptors (D1R and D5R) couple to stimulatory $G_{s/olf}$, whereas D2-class receptors (D2R, D3R, and D4R) couple to inhibitory $G_{i/o}$.[1] In terms of signalling, dopamine binding leads to a conformational change, allowing the G-protein α-subunit to trade guanosine diphosphate for guanosine triphosphate.[11] Subsequently, the operational α-subunit activates or inhibits its target protein, the enzyme adenylate cyclase (Figure 1.3). In the case of D1-class receptors, the operational AC catalyzes the conversion of adenosine triphosphate to cyclic adenosine monophosphate (cAMP), a secondary messenger that galvanizes versatile effectors such as protein kinase A.[3] Contrastingly, D2-class receptors inhibit AC and cAMP production in favour of G-protein-coupled inwardly rectifying potassium channel (GIRK) activation.[1,12] The resulting downstream signalling cascades from D1 and D2 receptors regulate calcium and potassium ion channels, respectively, thereby managing neuronal polarization and dopaminergic signalling.[1,4,12]

Additionally, regional distribution differs between the classes, with more distinct localization patterns observed on the receptor level. The D1-class is ubiquitous throughout the prefrontal cortex (PFC), substantia nigra as well as the striatum, more specifically within the caudate putamen and nucleus accumbens.[13–15] Similarly, the D2-class is expressed in the nucleus accumbens and olfactory tubercle, but also the hippocampus and frontal cortex to a lesser degree.[13,16] As a whole, both receptor classes ultimately contribute to memory and locomotion along the associated mesocorticolimbic and nigrostriatal circuits.[13]

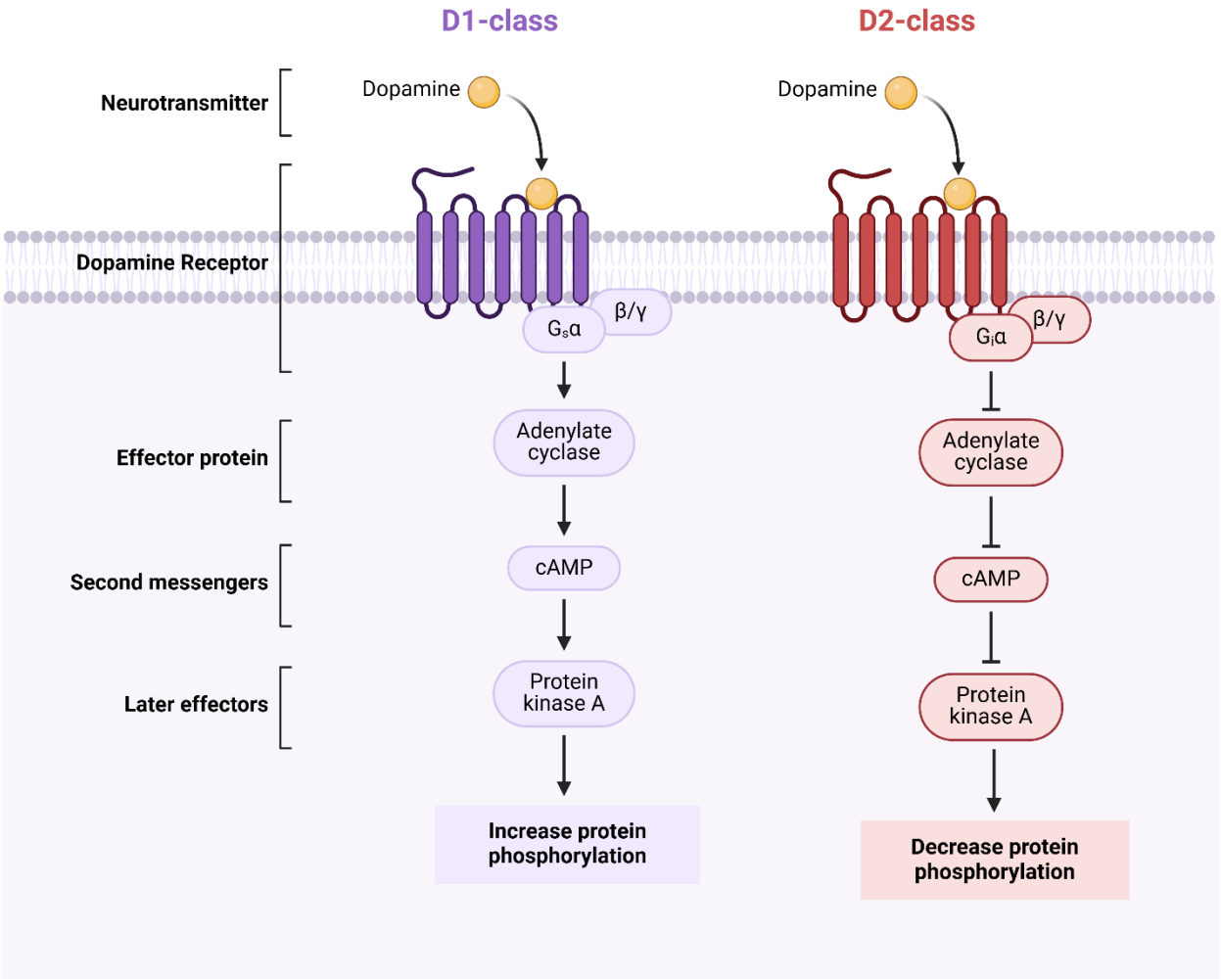

Figure 1.3. Overview of Dopaminergic Receptor Signalling Pathways. Dopamine receptors are GPCRs split into two classes, D1 and D2, based on whether cAMP production is stimulated or inhibited. Adapted from BioRender.

1.4. The Dopamine D1 Receptor

The dopamine D1 receptor (D1R) is widely recognized as the most populous dopaminergic receptor in the brain.[1,3,13,15,17] In terms of profile, D1R shares considerable structural homology with D5R, though the latter maintains greater dopamine affinity and adenylate cyclase activity.[13] Notably, D1R signal transduction and associated behavioural outcomes are determined by receptor situation. In the mesocorticolimbic pathway, D1R is expressed on PFC postsynaptic pyramidal neurons, facilitating depolarization and excitatory neurotransmission. [18–20] Although the precise role of the receptor in memory demands further elucidation, computational models indicate that D1R activity promotes such "high activity states" by enhancing the signal-to-noise ratio in favour of working memory rather than "distracting" stimuli.[21,22] Similarly, dopamine D1 receptors on nigrostriatal medium spiny neurons modulate excitatory responses along the "direct" circuit associated with voluntary action, such as movement.[13,23,24] As a whole, assessing the relative distribution of D1R offers insight into the performance of these functions.

1.5. Clinical Relevance

Clinically, D1R dysfunction is implicated in prevalent neurological conditions, with schizophrenia (SCZ) and Parkinson's disease (PD) among the more widely studied.[3] Although both conditions maintain distinct pathologies, they converge in terms of dopaminergic irregularities. In schizophrenia, a disequilibrium between D1R and D2R activity is suspected to trigger the host of positive and negative symptoms, with deficiencies in cortical D1R signalling associated with the latter.[25] For Parkinson's disease, the death of dopaminergic neurons reduces striatal dopamine levels, heightening D1R sensitivity and producing excessive behavioural outcomes.[26] Within such disease contexts, D1R represents a valuable clinical target as an abundant dopamine signalling element.

1.5.1. Schizophrenia

Schizophrenia is a neuropsychiatric condition that affects approximately 0.5-0.8% of people across the world.[27] Characterized by hallucinations, delusions, and anhedonia, the disorder commonly manifests between late adolescence and early adulthood. From an aetiological standpoint, the classical dopamine hypothesis posits that mesolimbic dopaminergic hyperactivity is responsible for positive psychosis, whereas hypoactivity correlates with negative psychosis.[18,28] Although mounting proof also insinuates a genetic basis affecting *N*-methyl-D-aspartate receptors, dopaminergic dysfunction remains a key pathophysiological and therapeutic target.[5,20] Given the preponderance of D1R in the prefrontal cortex, numerous studies have investigated the relationship between receptor stimulation and working memory performance, a common assessment of SCZ-associated cognitive deficits.[29–31] Treatment with higher doses of D1R agonists and antagonists triggered poor task execution relative to lower doses, revealing "inverted U-shaped" curves.[18,19,32,33] As such, this data demonstrates the correlation between disrupted D1R homeostasis and schizoid negative symptoms.

1.5.2. Parkinson's Disease

Parkinson's disease is a neurodegenerative condition marked by bradykinesia, tremors, and motor dysfunction.[6] As a highly pervasive disorder amongst elderly populations, the pathology involves widespread depletion of dopaminergic neurons in the substantia nigra, a key region in the nigrostriatal pathway for producing dopamine and regulating movement.[4] Levodopa is a common treatment for Parkinson's disease given its compensatory effect for lower endogenous dopamine levels. Though L-DOPA initially improves locomotion, its relationship with D1R has been correlated with increased receptor expression and overstimulation; the paucity of dopamine in this disease-state sensitizes the receptor to agonist interactions.[26,34] In terms of behavioural responses,

this eventually translates to a loss of motor control with prolonged use, as evinced by exacerbated dyskinesia.[34] Similarly, the administration of D1R agonists has exhibited antiparkinsonian effects, but dyskinesia is observed shortly thereafter.[3,35] As a whole, these observations articulate the link between D1R stimulation and parkinsonism.

1.6. Positron Emission Tomography and the Dopamine D1 Receptor

Positron emission tomography (PET) is a molecular imaging technique that enables visualization of receptor distribution in a living organism (Figure 1.4).[9] This non-invasive modality employs radiotracers, which are often established ligands modified to incorporate radionuclides such as carbon-11 (^{11}C) and fluorine-18 (^{18}F). Typically, the unstable radioisotope undergoes β^+ decay to release positrons that engage with electrons in an annihilation event, resulting in gamma photon emission detectable by the PET scanner.[36] The device then executes tomographic calculations to produce a spatial representation of the radiation signature, corresponding to radioligand binding and metabolism. In so doing, PET provides insight into specific binding of the tracer, which is extrapolated as a measure of regional receptor distribution and occupancy.[37]

In respect to D1R imaging, positron emission tomography is primarily used to interrogate receptor density in clinical populations. Schizophrenia and Parkinson's disease are relevant cases given the afflicted dopaminergic pathways are influenced by D1R activity, as illustrated by the inverted U-shaped dose-response curve and choreic dyskinesia following pharmacological challenge, respectively.[18,32,34,35] Correspondingly, PET enables visualization of regional D1R distribution, providing pathophysiological insight into the living brain of patients. Over the past several decades, numerous imaging studies have investigated the relative spatiality of the dopamine D1 receptor in SCZ and PD, with antagonist radioligands [^{11}C]SCH23390 and

[^{11}C]NNC112 being the traditional molecular probes.[38–42] Nevertheless, increasing evidence reveals inconsistent binding profiles and suboptimal selectivity.[33,38–41,43–47]

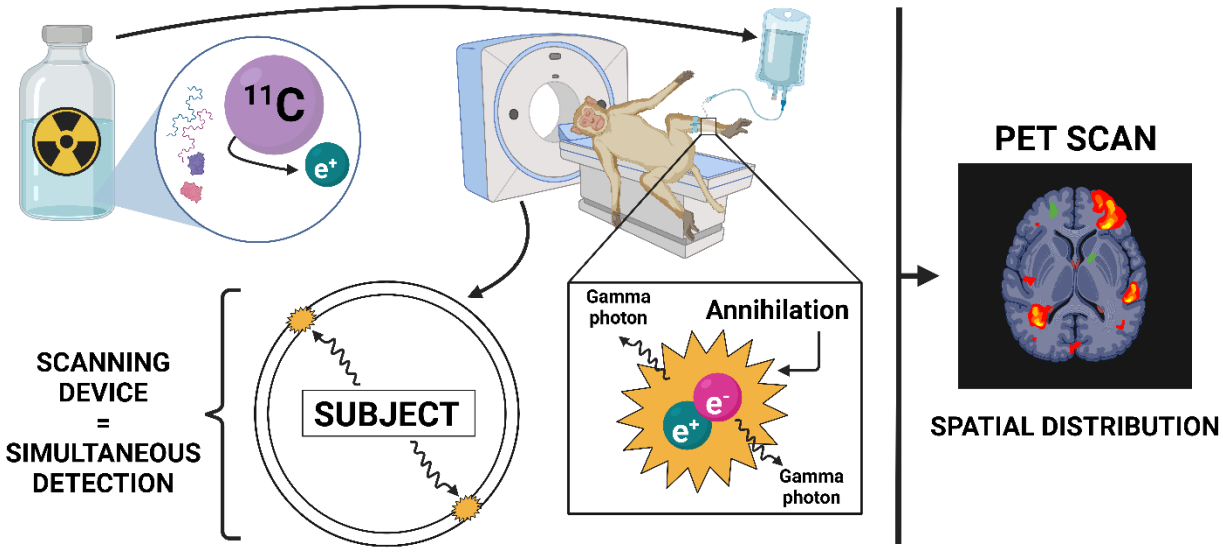

Figure 1.4. Summary of Positron Emission Tomography. PET is a molecular imaging technique that enables visualization of biological targets *in vivo.* As the radiotracer decays, gamma photons are detected by the scanner to produce a spatial representation of the signal, thereby depicting target density and distribution. Adapted from BioRender.

1.6.1. [^{11}C]SCH23390

SCH23390 ((5*R*)-8-chloro-3-methyl-5-phenyl-2,3,4,5-tetrahydro-1*H*-3-benzazepin-7-ol) is a benzazepine initially characterized as a D1R antagonist in the early 1980s.[48] Later in the decade, this compound was radiolabelled with carbon-11 to produce [^{11}C]SCH23390, becoming one of the first D1R radiotracers.[49,50] The radioligand was therefore used to investigate receptor distribution in schizophrenia and Parkinson's disease. However, several disparities were observed between studies. Pertaining to schizophrenia, clinical investigations examining cortical binding have alternately found baseline and decreased binding potential when comparing drug-naïve and drug-free SCZ patients to healthy controls.[42,47] Consequently, the regional density of D1R in the living schizoid brain remains unclear.

In Parkinson's disease, analogous inconsistencies are further exacerbated by a dearth of imaging studies.[51] When evaluating striatal D1R binding between striatonigral degeneration (SND) patients, PD patients, and healthy controls, there was negligible difference in quantitative distribution between the Parkinson's disease patients and baseline group.[38] Similarly, striatal D1R binding appeared consistent amongst PD patients despite varying degrees of dyskinesia.[46] While such results may undermine the pathophysiological significance of D1R, they are heavily contrasted by nonhuman primate MPTP (1-methyl-4-phenyl-1,2,3,6-tetrahydropyridine) models wherein Parkinsonism is chemically induced. For instance, a PET study revealed a decrease in striatal D1R binding amongst MPTP-lesioned primates, further confusing the correlation between receptor density and Parkinson's disease.[41]

1.6.2. [^{11}C]NNC112

NNC112 ((5*S*)-5-(1-benzofuran-7-yl)-8-chloro-3-methyl-1,2,4,5-tetrahydro-3-benzazepin-7-ol) is another benzazepine antagonist developed and radiolabelled as [^{11}C]NNC112 between the late 1990s and early 2000s.[52,53] Much like [^{11}C]SCH23390, the radiotracer was largely used within schizophrenia and Parkinson's disease contexts and showed similarly discrepant results. Notably, SCZ studies have illustrated both increases and baseline cortical [^{11}C]NNC112 binding when evaluating drug-naïve and drug-free patients relative to healthy controls.[33,54] In Parkinson's disease, however, striatal D1R density appeared similar to the control participants.[55] Though comparatively fewer clinical investigations have employed [^{11}C]NNC112, the imaging agent seems to display inconsistent binding profiles in disease.

1.6.3. Selectivity Issues

Given structural similarities between monoaminergic receptors, both [^{11}C]SCH23390 and [^{11}C]NNC112 have exhibited congruent selectivity problems, especially in relation to serotonin receptor 5-HT$_{2A}$.[44] Although insignificant in the striatum, off-target binding to 5-HT$_{2A}$ is appreciable in cortical regions. Interestingly, the compounds demonstrate greater selectivity for 5-HT$_{2A}$ than D1R within the living brain.[45] This was initially illustrated in 5-HT$_2$ competition studies in rats, wherein SCH23390 demonstrated higher affinity for the serotonergic receptor *in vivo* rather than *in vitro*.[56] Furthermore, according to 5-HT$_{2A}$ blocking studies and comparative receptor imaging, around 20-30% of [^{11}C]NNC112 binding is associated with 5-HT$_{2A}$.[43,57] While [^{11}C]SCH23390 has not been as thoroughly characterized, a preliminary profile appears analogous with around 25% of receptor availability representing 5-HT$_{2A}$ interactions.[44,45] As a whole, these results may recontextualize PET imaging results in SCZ, underscoring the necessity of prioritizing D1R selectivity in future radiotracers.[44,45]

1.7. D1R-Ligand Interactions

The initial series of 'selective' D1-class ligands maintained benzazepine cores, as represented by the chlorinated antagonists and catechol agonists: SCH23390, NNC112, SKF38393, and SKF82957, respectively (Figure 1.5).[58,59] Due to suboptimal pharmacokinetics and activity, benzazepines were retired as therapeutic agents, though SCH23390, NNC112, and SKF82957 were repurposed as molecular imaging probes. Ensuing iterations of D1R ligands forwent both benzazepines and antagonism in favour of catechol agonists.[58] While orthosteric binding stimulated D1R activity, representative compounds such as DHX and A-77636 eventually triggered receptor desensitization and internalization, becoming less effective with prolonged use.[60,61] Additionally, the catechol functionality contributed to deficiencies in bioavailability, further emphasizing the need for novel D1R targeting paradigms.[58]

1.7.1. Allosteric Modulation

Allosteric modulators bind to non-orthosteric, or allosteric sites on target receptors, which are regions revealed as the GPCR transitions between inactive and active forms.[3,58] In so doing, such ligands stabilize receptor conformations that translate to modulatory effects on orthosteric affinity and functional outcomes.[62] Positive allosteric modulators (PAMs) are increasingly popular therapeutic strategies for the dopamine D1 receptor, for they potentiate receptor activity in the presence of dopamine, presenting a "self-limiting" characteristic to reduce overstimulation and desensitization.[58] Non-orthosteric binding bypasses the catechol functionality, resulting in structural diversity and improved bioavailability amongst D1R PAMs. Furthermore, because allosteric sites are less conserved between receptors, such molecules demonstrate more target-selective binding profiles.[58] These attributes address the limitations of previous D1R therapeutics and imaging agents alike, offering a promising avenue for dopaminergic investigation.

1.8. D1R Positive Allosteric Modulator ASP4345

ASP4345 (2-(5-chloro-2-oxo-1,3-benzoxazol-3(2*H*)-yl)-*N*-{[5-(trifluoromethyl)-1*H*-benzimidazol-2-yl]methyl} acetamide hydrochloride) is a suspected D1R PAM developed by Astellas Pharma in 2014 (Figure 1.5).[63] Corresponding cAMP accumulation assays and rodent cognition studies revealed mild dopamine potentiation and improvements in spatial memory, suggesting an allosteric modulatory profile.[58,63] Initially proposed as a treatment for schizophrenia, ASP4345 was evaluated in phase I clinical trials, showing pharmacokinetics indicative of swift brain uptake.[64] However, the drug was removed from development when phase II trials failed to note improvements in cognitive efficacy for schizophrenia patients.[65] Despite such therapeutic shortcomings, ASP4345 warrants further exploration as a D1R radiotracer given its brain penetration, allosteric binding, and established safety in humans.

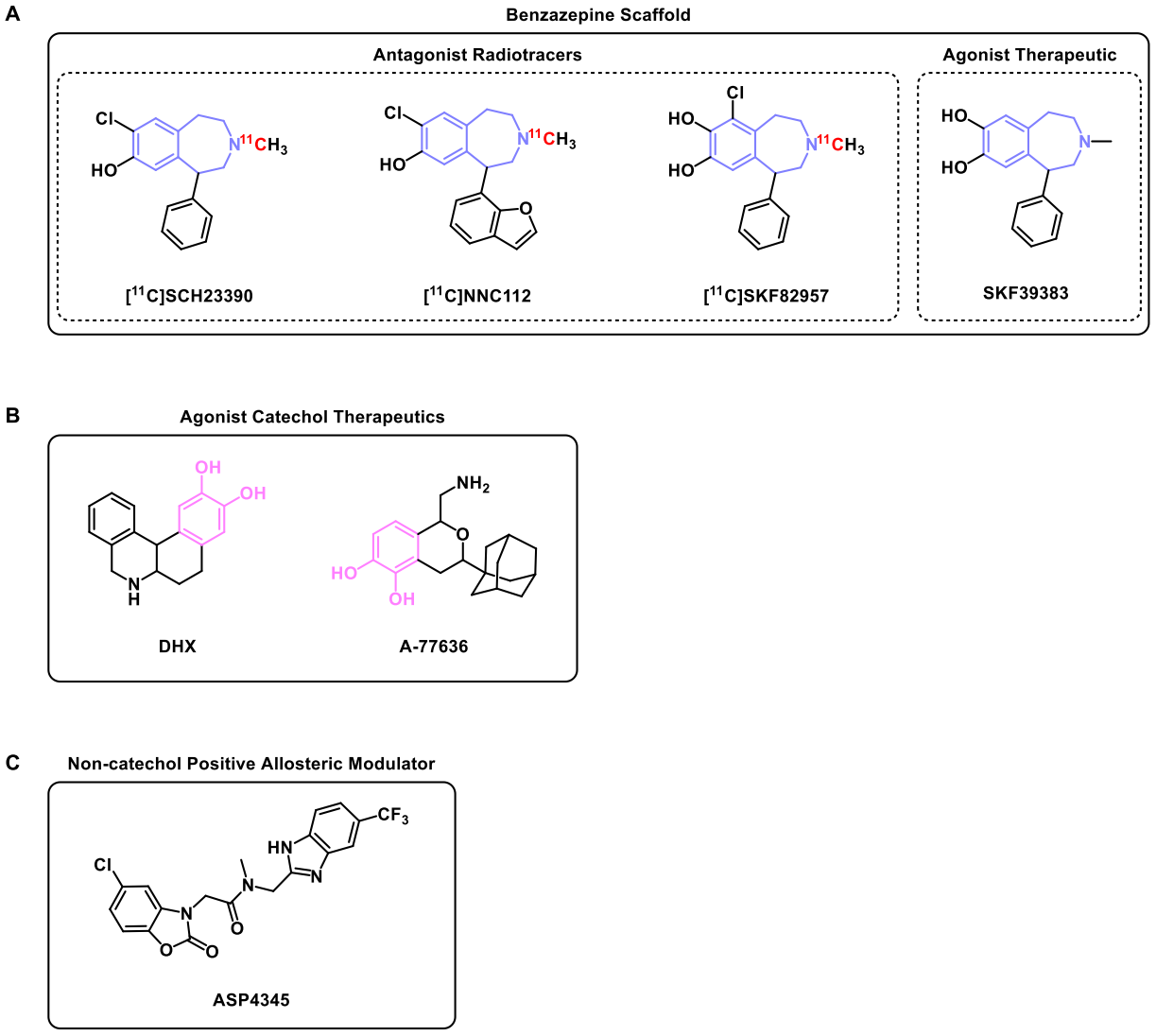

Figure 1.5. Dopamine D1 Receptor Ligands. (A) Benzazepine-based molecules SCH23390, NNC112, SKF82957, and SKF39383 represent the first generation of D1R ligands for either therapeutic or imaging applications. **(B)** Catechol agonist therapeutics DHX and A-77636 succeeded benzazepines as the next line of D1R drug candidates. **(C)** Astellas Pharma drug ASP4345 is a suspected positive allosteric modulator for the dopamine D1 receptor. Though ineffective as an SCZ therapeutic, ASP4345 may be repurposed as a molecular imaging agent.

1.9. Hypothesis and Objectives

Given its allosteric binding and brain penetrability, we hypothesize that ASP4345 presents a selective D1R radiotracer candidate to characterize receptor distribution in a living system. As such, we aim to synthesize and evaluate ASP4345 as an imaging agent for the dopamine D1 receptor based on the following objectives:

a. ASP4345 Synthesis: To synthesize ASP4345 based on procedures described by Astellas Pharma

b. *In Vitro* Pharmacological Characterization: To characterize the ligand-receptor interactions between ASP4345 and D1R activity using a luminescence-based cAMP accumulation assay

c. Radiolabelling Strategy Screening: To identify radiolabelling strategies based on precursor viability and radiosynthetic compatibility with ASP4345

Through these experimental approaches, we hope to construct a novel radiotracer development workflow, enabling greater understanding of D1R distribution in neurological conditions such as Parkinson's disease and schizophrenia.

CHAPTER II: MATERIALS AND METHODS

2.1. Materials

Unless otherwise specified, all chemical reagents were obtained from Sigma-Aldrich, TCI Chemicals, Thermo-Fisher Scientific, and Oakland Chemical. Nuclear magnetic resonance (NMR) experiments were performed using the Spinsolve 80 ULTRA (Magritek) and AVANCE II 400 (Bruker) instruments, with analysis using MestReNova software (Mestrelab Research). To monitor reactions, ultra-performance liquid chromatography-mass spectrometry (UPLC-MS) was carried out using the Xevo TQD (Waters) and MassLynx software (Waters). Additionally, thin-layer chromatography (TLC) was conducted using glass silica-coated plates (Sigma-Aldrich) to evaluate reaction progress.

2.2. ASP4345 Standard Synthesis: 2-(5-chloro-2-oxo-1,3-benzoxazol-3(2*H*)-yl)-*N*-{[5-(trifluoromethyl)-1*H*-benzimidazol-2-yl]methyl} acetamide hydrochloride

2.2.1. Synthesis of (5-chloro-2-oxo-1,3-benzoxazol-3(2*H*)-yl) acetic acid

To a round-bottom flask equipped with a magnetic stirrer, 5-chloro-1,3-benzoxazol-2(3*H*)-one (2.95 mmol, 500 mg) and acetone (7.5 mL) were added (Figure 2.1A). Next, potassium carbonate (4.42 mmol, 611 mg) and *tert*-butyl bromoacetate (3.54 mmol, 0.52 mL) were incorporated, whereupon the mixture was stirred under argon gas and reflux (60 °C) for 1.5 hours. After confirming reaction completion, the mixture was filtered and washed with acetone. The filtrate was then collected and condensed under reduced pressure, after which the resulting solid was washed with a solution of hexanes and ethyl acetate (6:1) followed by water. Subsequent vacuum-drying yielded the solid white crystalline product **1a**, *tert*-butyl (5-chloro-2-oxo-

1,3,benzoxazole-3(2*H*)-yl) acetate (638 mg, 76% yield). Characterization data is in accord with literature reports.[63]

^{1}H-NMR (80 MHz, DMSO-d6): δ 7.47 (d, 1H, *J* = 2.0 Hz), 7.36 (d, 1H, *J* = 8.70 Hz), 7.13 (dd, 1H, *J* = 8.50, 2.0 Hz), 4.59 (s, 2H), 1.36 (s, 9H) ppm

For the deprotection reaction, **compound 1a** (1.64 mmol, 465 mg) was dissolved in dichloromethane (1.5 mL), whereupon trifluoracetic acid (19.6 mmol, 1.5 mL) was added. The mixture was then stirred under argon at room temperature overnight. After confirming reaction completion by TLC, the mixture was condensed under reduced pressure and washed with water before filtration. Such yielded the solid white product **1b**, (5-chloro-2-oxo-1,3-benzoxazol-3(2*H*)-yl) acetic acid (231 mg, 62% yield). Characterization data is in accord with literature reports.[63]

^{1}H-NMR (80 MHz, DMSO-d6): δ 7.49 (d, 1H, *J* = 5.60 Hz), 7.35 (d, 1H, *J* = 10.40 Hz), 7.17 (d, 1H, *J* = 2.40 Hz), 4.63 (s, 2H) ppm

2.2.2. Synthesis of *N*-methyl-1-[5-(trifluoromethyl)-1*H*-benzimidazol-2-yl] methanamine dihydrochloride

In a round-bottom flask equipped with a magnetic stirrer, *N*-(tert-butoxycarbonyl)-*N*-methylglycine (3.09 mmol, 585 mg) was dissolved in a mixture of triethylamine (4.94 mmol, 0.69 mL) and tetrahydrofuran (7.1 mL) (Figure 2.1B). *n*-Butyl chloroformate (4.33 mmol, 0.56 mL) was then added under ice-cooling and the reaction was stirred under argon gas at room temperature for 1 hour. Next, the mixture was filtered and washed with tetrahydrofuran. The resulting filtrate was combined with 4-(trifluoromethyl)benzene-1,2-diamine (3.09 mmol, 546 mg) under ice-cooling and stirred under argon gas at room temperature overnight. Upon verifying reaction completion via TLC, the mixture was condensed under reduced pressure and purified via silica

column chromatography using an eluent system of ethyl acetate and hexanes (2:1). Subsequently, acetic acid (5.0 mL) was added to the residue, whereupon it was stirred at 80 °C for 2.5 hours. Once again, substrate conversion was assessed using TLC before allowing the mixture to cool and evaporated *in vacuo*. To purify, column chromatography was performed using 2:1 ethyl acetate/hexanes. Residual ethyl acetate was removed from the isolated fractions using chloroform and condensed under reduced pressure. This final evaporation step yielded the brown solid product **2a**, *tert*-butylmethyl{[5-(trifluoromethyl)-1*H*-benzimidazol-2-yl]methyl} carbamate (556 mg, 55% yield). Characterization data is in accord with literature reports.[63]

^{1}H-NMR (80 MHz, $CDCl_3$): δ 7.89 (d, 1H, *J* = 5.40 Hz), 7.74 (d, 1H, *J* = 5.10 Hz), 7.58 (dd, 1H, *J* = 1.20, 0.8 Hz), 1.75 (s, 2H), 2.99 (s, 3H), 1.50 (s, 9H) ppm

For the deprotection reaction, **compound 2a** (1.22 mmol, 400 mg) was combined with 4 M hydrochloric acid in dioxane (8 mL) and stirred under argon gas at room temperature for 2 hours. After ensuring substrate conversion, the mixture was triturated severally in diethyl ether before evaporation *in vacuo*. Such yielded the solid tan product **2b**, *N*-methyl-1-[5-(trifluoromethyl)-1*H*-benzimidazol-2-yl] methanamine dihydrochloride (343 mg, 93% yield). Characterization data is in accord with literature reports.[63]

^{1}H-NMR (80 MHz, DMSO-d6): δ 7.81 (d, 1H, *J* = 8.70 Hz), 7.59 (d, 1H, *J* = 7.70 Hz), 7.43 (d, 1H, *J* = 9.20 Hz), 4.32 (s, 2H), 2.31 (s, 3H) ppm

2.2.3. Coupling of (5-chloro-2-oxo-1,3-benzoxazol-3(2*H*)-yl) acetic acid and *N*-methyl-1-[5-(trifluoromethyl)-1*H*-benzimidazol-2-yl] methanamine dihydrochloride

To a round-bottom flask equipped with a magnetic stirrer, **compounds 1b** (0.724 mmol, 165 mg) and **2b** (0.794 mmol, 240 mg) were dissolved in dichloromethane (5.5 mL) (Figure 2.1C).

Next, triethylamine (2.25 mmol, 0.31 mL), hydroxybenzotriazole (0.873 mmol, 118 mg), and 1-ethyl-3-(3-dimethylaminopropyl)carbodiimide (0.860 mmol, 165 mg) were added and the mixture was stirred under argon at room temperature overnight. Once reaction completion was assessed using TLC, a work-up was performed by diluting with ethyl acetate and washing with water (3 x 10 mL), aqueous sodium bicarbonate solution (3 x 10 mL), and brine (2 x 10 mL). The combined organic layers were then dried over magnesium sulfate and evaporated *in vacuo*. Subsequently, the resulting solid was combined with 4 M hydrochloric acid in dioxane (0.48 mL) and stirred at room temperature under argon for 1 hour. The mixture was triturated severally in diethyl ether before condensing under reduced pressure, yielding the final ivory solid, 2-(5-chloro-2-oxo-1,3-benzoxazol-3(2*H*)-yl)-*N*-{[5-(trifluoromethyl)-1*H*-benzimidazol-2-yl]methyl} acetamide hydrochloride (248 mg, 86%), referred to as ASP4345. Characterization data is in accord with literature reports.[63]

^{1}H-NMR (400 MHz, DMSO-d6): δ 8.05 (d, 1H, *J* = 10.70 Hz), 7.88 (d, 1H, *J* = 9.20 Hz), 7.70 (d, 1H, *J* = 9.80 Hz), 7.61 (dd, 1H, *J* = 2.10, 15.50 Hz), 7.44 (dd, 1H, *J* = 8.50, 11.00 Hz), 7.23 (ddd, 1H, *J* = 2.20, 8.50, 17.60 Hz), 5.04 (d, 2H, 10.50 Hz), 4.94 (s, 2H), 3.33 (s, 3H) ppm

MS (ESI+, m/z): calculated [M+H]+ $C_{19}H_{14}ClF_3N_4O_3$ as 439.1, found as 439.1

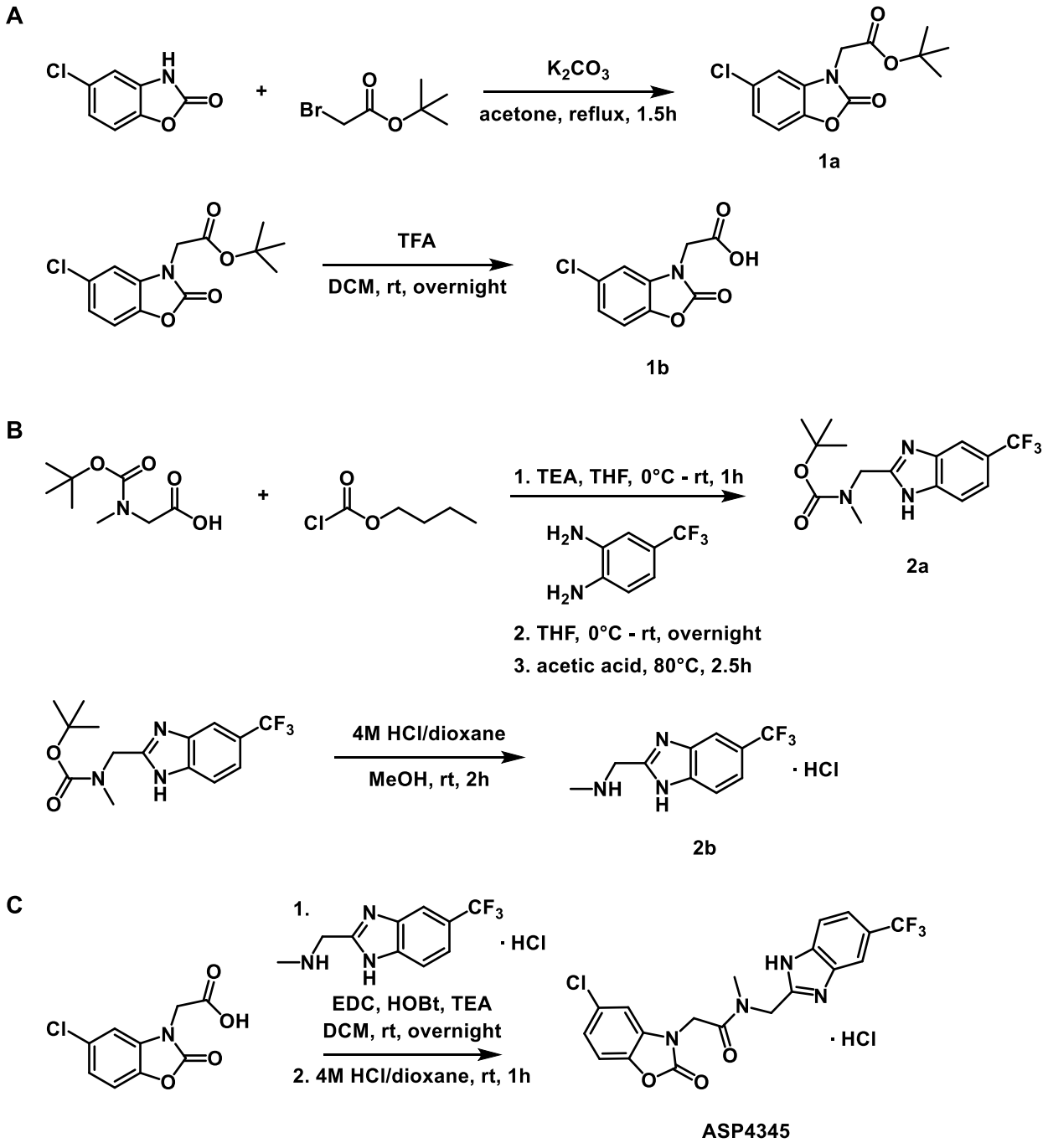

Figure 2.1. Synthesis of ASP4345. As detailed by Astellas Pharma, ASP4345 is produced through a five-step synthesis in which oxazolidinone 1b is coupled to imidazole 2b, forming ASP4345 in 86% yield.

2.3. GloSensor Assays

HEK293T-Glo were co-transfected with plasmid constructs for human D1R (hD1R), rat D1R (rD1R), and rat D5R (rD5R) using jetPRIME® (Polyplus) following the manufacturer protocol. On the following day, cells were split and seeded using starvation media (DMEM with 1% FBS and 1% penicillin-streptomycin) onto Poly-L-Lys (PLL) coated 384-well cell culture plates, at a density of 30 000 cells per well and total volume of 40 μL, before overnight incubation at 37 °C. Next, media was expelled from the cell plate and 20 μL of HBSS (20 mM HEPES, 1× Hanks' balanced salt solution, pH 7.40) and 1 mg/mL luciferin solution (GoldBio) was added to each well prior to 30-minute incubation in the dark.

Corresponding drug plates were prepared for each experiment using stock solutions of 10 mM dopamine, ASP4345, and MLS1082 in DMSO; each drug was serially diluted at 5X-6X of the final concentration (0 to 10 μM). After a 10-minute incubation in the dark, both cell and drug plates were loaded onto the FLIPR high-throughput cellular screening system (Molecular Devices) to transfer drugs to cells plate, with 5 μL of the allosteric modulators added to the cells 10 minutes before a 5 μL addition of the agonists. Once the treated cells were incubated in the dark for another 10 minutes, luminescence was detected and quantified using a Hidex Sense Beta Plus (Gamble Technologies). The resulting data was plotted and analyzed using GraphPad Prism 10 (Dotmatics).

2.4. Radiolabelling Strategy Screening

2.4.1. $[^{11}C]CO_2$ Fixation Aminophenol Precursor

i. Methyl Ether Protected Precursor

To a solution of 5-chloro-2-methoxyaniline (6.36 mmol, 1 g), *N*,*N*-diisopropylethylamine (12.7 mmol, 2.2 mL) and acetonitrile (12.8 mL) was slowly added *tert*-butyl bromoacetate (9.54

mmol, 1.5 mL). The reaction was stirred under argon gas at 60 °C until majority substrate conversion after 6 hours. To purify the residue, column chromatography was performed using 1:5 diethyl ether/hexanes. The isolated fractions were condensed under reduced pressure to reveal the yellow oil product, 2-methyl-2-propanyl-*N*-(5-chloro-2-methoxyphenyl) glycinate (821 mg, 47% yield).

^{1}H-NMR (80 MHz, DMSO-d6): δ 6.70 (d, 1H, *J* = 8.40 Hz), 6.55 (d, 1H, *J* = 2.40 Hz), 6.31 (d, 1H, *J* = 2.30 Hz), 3.96 (s, 2H), 3.76 (3H, 5.70 Hz), 1.35 (s, 9H) ppm

MS (ESI+, m/z): calculated [M+H]+ $C_{13}H_{18}ClNO_3$ as 272.1, not found, calculated fragment [M+H]+ C_8H_9ClNO as 170.0, found as 169.9

To cleave the *tert*-butyl protecting group, 2-methyl-2-propanyl-*N*-(5-chloro-2-methoxyphenyl) glycinate (3.00 mmol, 815 mg) was dissolved in dichloromethane (2 mL), whereupon trifluoracetic acid (36.0 mmol, 2.7 mL) was added. The mixture was then stirred under argon at room temperature overnight. After confirming reaction completion by TLC, the mixture was condensed under reduced pressure and washed with water before filtration. Such yielded the solid tan product, *N*-(5-chloro-2-methoxyphenyl) glycine (201 mg, 31% yield).

MS (ESI+, m/z): calculated [M+H]+ $C_9H_9ClNO_3$ as 216.0, not found, calculated fragment [M+H]+ C_8H_8ClNO as 170.0, found as 170.0

For amide bond formation, *N*-methyl-1-[5-(trifluoromethyl)-1*H*-benzimidazol-2-yl] methanamine dihydrochloride (0.270 mmol, 81 mg) was dissolved in dichloromethane (2.9 mL). To this solution was added triethylamine (0.810 mmol, 0.12 mL), hydroxybenzotriazole (0.330 mmol, 45 mg), and 1-ethyl-3-(3-dimethylaminopropyl)carbodiimide (0.330 mmol, 63 mg). Next, *N*-(5-chloro-2-methoxyphenyl) glycine (0.270 mmol, 60 mg) was incorporated slowly before the

reaction was stirred under argon at room temperature for 4 hours. After assessing reaction completion via TLC and UPLC, a work-up was performed by diluting with ethyl acetate and washing with water (3 x 5 mL), aqueous sodium bicarbonate solution (3 x 5 mL), and brine (2 x 5 mL). The combined organic layers were then dried over magnesium sulfate and evaporated *in vacuo*. Subsequently, the resulting solid was combined with 4 M hydrochloric acid in dioxane (0.35 mL) and stirred at room temperature under argon for 1 hour. Again, the mixture was diluted with ethyl acetate and washed with water (3 x 5 mL), whereupon the collected organic layers were dried over magnesium sulfate and condensed under reduced pressure. Overall, such yielded the brown oil product, *N*-{[5-(trifluoromethyl)-1*H*-benzimidazol-2-yl]methyl}-2-[(5-chloro-2-methoxyphenyl)amino]-*N*-methylacetamide (110 mg, 95% yield).

MS (ESI+, m/z): calculated $[M+H]+$ $C_{19}H_{18}ClF_3N_4O_2$ as 427.1, found as 427.2

To deprotect the phenol, *N*-{[5-(trifluoromethyl)-1*H*-benzimidazol-2-yl]methyl}-2-[(5-chloro-2-methoxyphenyl)amino]-*N*-methylacetamide (0.234 mmol, 100 mg) was added to a solution of lithium chloride (0.938 mmol, 40 mg) and dimethylformamide (2 mL). The reaction mixture was stirred under argon gas at 100°C overnight. After quenching with aqueous 10% lithium chloride solution, the reaction mixture was washed with ethyl acetate (3 x 10 mL) and brine (2 x 10 mL), whereupon the combined organic layers were dried over magnesium sulfate and condensed under reduced pressure.

Alternative Methyl Ether Deprotection Conditions

a. Nucleophilic

To a mixture of 5-chloro-2-methoxyaniline (0.317 mmol, 50 mg) and sodium hydroxide (0.951 mmol, 38 mg) was added *N*-methyl-2-pyrrolidone (3.2 mL) and *tert*-butyl

thiol (0.476 mmol, 0.05 mL). The reaction was stirred under argon gas at 130 °C for 3 hours with substrate conversion monitored via TLC. Subsequently, the mixture was allowed to cool to room temperature, whereupon it was acidified with aqueous 1N HCl added dropwise. A work-up was then performed by diluting with ethyl acetate and washing with water (3 x 5 mL) and brine (2 x 5 mL) before drying over magnesium sulfate followed by evaporation *in vacuo*.

To a solution of sodium hydride (0.130 mmol, 3 mg), hexamethylphosphoramide (0.130 mmol, 0.02 mL), and xylene (0.15 mL), *N*-methylaniline (0.130 mmol, 0.01 mL) was added dropwise. The mixture was then stirred under argon at 65 °C, whereupon 5-chloro-2-methoxyaniline (0.060 mmol, 10 mg) was incorporated and the reaction temperature raised to 85 °C for 30 minutes.

b. Lewis Acid

To a solution of aluminum chloride (0.015 mmol, 2 mg) and acetonitrile was added 5-chloro-2-methoxyaniline (0.060 mmol, 10 mg). The resulting mixture was stirred under argon at 70 °C for 30 minutes.

To a solution of dichloromethane (0.66 mL) and acetonitrile (0.44 mL) was added 5-chloro-2-methoxyaniline (0.060 mmol, 10 mg). Next, boron trifluoride etherate (0.100 mmol, 0.01 mL) and aluminum chloride (0.600 mmol, 80 mg) were incorporated, and the resulting mixture was stirred under argon at 0 °C for 30 minutes.

c. Brønsted Acid

To a solution of concentrated sulfuric acid (0.40 mL) was added 5-chloro-2-methoxyaniline (0.060 mmol, 10 mg). The mixture was stirred under argon at 70 °C for 30 minutes.

To a solution of sodium iodide (0.070 mmol, 11 mg) and 45% w/v hydrobromic acid (0.67 mL) was added 5-chloro-2-methoxyaniline (0.060 mmol, 10 mg). The mixture was stirred under argon at 90 °C for 30 minutes.

ii. Benzyl Ether Protected Precursor

Adapting a previous procedure, to a solution of potassium carbonate (0.618 mmol, 86 mg) and acetone (1.9 mL) was added benzyl bromide (0.464 mmol, 0.06 mL) and 5-chloro-2-aminophenol (0.696 mmol, 100 mg). The resulting mixture was stirred under argon and reflux (60 °C) for two hours. After confirming reaction completion using TLC, a work-up was performed by washing with ethyl acetate (3 x 10 mL), 10% sodium hydroxide solution (3 x 10 mL) and brine (2 x 10 mL), whereupon the collected organic layers were dried over magnesium sulfate and condensed under reduced pressure. Next, the residue was purified using column chromatography with an eluent system of 2:1 diethyl ether/hexanes. The relevant fractions were isolated and evaporated *in vacuo* to produce the product, 2-(benzyloxy)-5-chloroaniline (4 mg, 4% yield). Characterization data is similar to literature reports.[66]

MS (ESI+, m/z): calculated $[M+H]^+$ $C_{13}H_{12}ClNO$ as 234.1, found as 234.0

To cleave the benzyl ether, 10% palladium on carbon catalyst (0.002 mmol, 0.2 mg) was added to a flask evacuated with argon. Subsequently, a solution of 2-(benzyloxy)-5-chloroaniline (0.008 mmol, 2 mg) and methanol (1 mL) was incorporated. The flask was again thoroughly

evacuated by applying a vacuum to flush out residual air and attaching a balloon filled with hydrogen gas before vigorous stirring at room temperature for 24 hours.

iii. Methoxyethoxy methyl ether Protected Precursor

To a solution of 5-chloro-2-aminophenol (0.350 mmol, 50 mg), *N*,*N*-diisopropylethylamine (0.530 mmol, 0.09 mL), and dichloromethane (5 mL) was slowly added 2-methoxyethoxymethyl chloride (0.530 mmol, 0.06 mL). The reaction was then stirred under argon gas at room temperature for 4 hours. After washing with water (3 x 10 mL), sodium hydroxide solution (3 x 10 mL) and brine (2 x 10 mL), the mixture was dried over magnesium sulfate and evaporated *in vacuo*.

Alternative Methoxyethoxy methyl ether Installation Conditions

a. Sodium Hydride Based Installation

To a solution of 5-chloro-2-aminophenol (0.035 mmol, 5 mg), sodium hydride (0.063 mmol, 1.5 mg), and tetrahydrofuran (0.2 mL) was slowly added 2-methoxyethoxymethyl chloride (0.081 mmol, 0.01 mL). The resulting mixture was then stirred at 0 °C for 30 minutes.

b. Tetrabutylammonium Bromide Based Installation

To a mixture of 5-chloro-2-aminophenol (0.035 mmol, 5 mg), tetrabutylammonium bromide (0.007 mmol, 2 mg) and 40% w/v sodium hydroxide/dichloromethane solution (0.6 mL) was slowly added 2-methoxyethoxymethyl chloride (0.081 mmol, 0.01 mL). The resulting mixture was then stirred at 0 °C for 30 minutes.

2.4.2. Cu-mediated ^{18}F-Fluorination

To prepare the K_{222}/K_2CO_3 solution, Kryptofix 222 (15 mg) and potassium carbonate (3 mg) were added to a 1 mL mixture of acetonitrile (0.8 mL) and water (0.2 mL). Next, [^{18}F]fluoride (~ 222 MBq) was syringed through a Sep-Pak Accell Plus QMA cartridge (Waters) conditioned with sterile water and sodium bicarbonate before being flushed with air. The K_{222}/K_2CO_3 mixture was passed through the same cartridge into receiving V-vials, whereupon the resulting [^{18}F]KF/K_{222} solution was dried under nitrogen gas, iterative additions of acetonitrile (3 x 1 mL), before being dissolved in anhydrous DMF. To each reaction vial containing tetrakis(pyridine)copper (II) triflate (0.03 mmol, 20 mg) and 4-(4,4,5,5-tetramethyl-1,3,2-dioxaborolan-2-yl) benzonitrile (0.02 mmol, 5 mg), the [^{18}F]KF/K_{222} solution (~ 6 MBq, 50 μL) was added with DMF (300 μL). For the screening reactions, ASP4345 (0.02 mmol, 10 mg) in DMF (300 μL) was added immediately after the radioactivity. The mixtures were then stirred at 110 °C for 20 minutes. After quenching with water, aliquots from each reaction were spotted on TLC plates and eluted with ethyl acetate. Lastly, each plate was subsequently scanned and analyzed using the Bioscan AR-2000 detector (Eckert & Ziegler).

2.4.3. Synthesis of ^{11}C-Methylation Acetamide Model Substrates

Model Precursor: Synthesis of N-benzylacetamide

To a solution of triethylamine (4.80 mmol, 0.66 mL) and ethyl acetate (8 mL) was added benzylamine (4.00 mmol, 0.44 mL) followed by acetic anhydride (4.8 mmol, 0.44 mL). The reaction was then stirred under argon gas at room temperature for 30 minutes. After confirming substrate conversion via TLC, a work-up was performed by diluting with ethyl acetate and washing with aqueous 1 M HCl (3 x 10 mL), aqueous sodium bicarbonate solution (3 x 10 mL), and brine (2 x 10 mL). The combined organic layers were then dried over magnesium sulfate and evaporated

in vacuo. Such yielded the white solid product, *N*-benzylacetamide (422 mg, 71% yield). Characterization data is in accord with literature reports.[67]

^{1}H-NMR (80 MHz, DMSO-d6): δ 7.28 (s, 5H), 4.26 (d, 2H, *J* = 5.80 Hz), 1.90 (s, 3H) ppm

Model Standard: Synthesis of N-benzyl-N-methylacetamide

To a solution of triethylamine (4.80 mmol, 0.66 mL) and ethyl acetate (8 mL) was added *N*-methylbenzylamine (4.00 mmol, 0.52 mL) followed by acetic anhydride (4.8 mmol, 0.44 mL). The reaction was then stirred under argon gas at room temperature for 30 minutes. After confirming substrate conversion via TLC, a work-up was performed by diluting with ethyl acetate and washing with aqueous 1 M HCl (3 x 10 mL), aqueous sodium bicarbonate solution (3 x 10 mL), and brine (2 x 10 mL). The combined organic layers were then dried over magnesium sulfate and evaporated *in vacuo*. Such yielded the white solid product, *N*-benzyl-*N*-methylacetamide (438 mg, 67% yield). Characterization data is in accord with literature reports.[68]

^{1}H-NMR (80 MHz, DMSO-d6): δ 7.24 (s, 5H), 4.58 (d, 2H, *J* = 5.50 Hz), 3.11-2.72 (m, 3H), 2.12 (s, 3H) ppm

CHAPTER III: RESULTS

3.1. Synthesis of ASP4345

ASP4345 was produced in a five-step synthesis and characterized via NMR based on procedures established by Astellas Pharma (see Figure 2.1).[63] To this end, (5-chloro-2-oxo-1,3-benzoxazol-3(2*H*)-yl) acetic acid was generated by an amine alkylation followed by a *tert*-butyloxycarbonyl (Boc) deprotection reaction, achieving a 76% yield. Similarly, *N*-methyl-1-[5-(trifluoromethyl)-1*H*-benzimidazol-2-yl] methanamine dihydrochloride was synthesized from an acyl substitution followed by another Boc deprotection, forming the product in 93% yield. For the final step, (5-chloro-2-oxo-1,3-benzoxazol-3(2*H*)-yl) acetic acid and *N*-methyl-1-[5-(trifluoromethyl)-1*H*-benzimidazol-2-yl] methanamine dihydrochloride underwent a coupling reaction using 1-ethyl-3-(3-dimethylaminopropyl)carbodiimide as an activating agent, producing 248 mg of ASP4345 in 86% yield.

3.2. *In vitro* Pharmacological Characterization with GloSensor

The GloSensor assay exploits modified firefly luciferase as a cAMP-responsive biosensor that oxidizes D-luciferin substrate into luminescent oxyluciferin.[69] Such defines cAMP accumulation as a function of G_s-coupled GPCR activation, with increasing luminescence correlated with receptor stimulation (Figure 3.1). The experiment is performed with HEK293T cells stably expressing the engineered luciferase, after which co-transfection introduces the GPCR of interest. At this point, ligands can be tested in various concentrations and correlated with relative luminescence units (RLUs) as a measure of cAMP accumulation. Hence, this assay offers insight into the interactions between D1R, a G_s-coupled GPCR, and ASP4345, a suspected PAM.

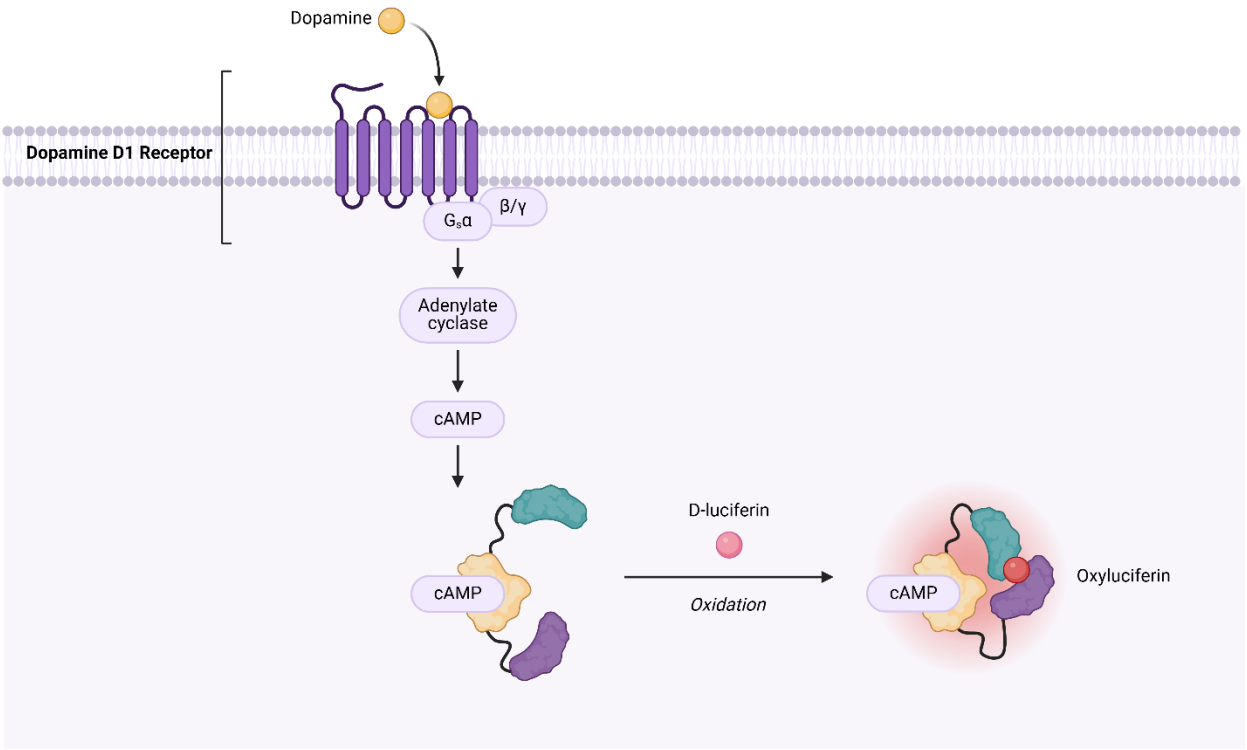

Figure 3.1. Illustration of the GloSensor Assay. GloSensor is a luciferase-based assay that reflects GPCR activity as a measure of cAMP levels. When D1R is stimulated, cAMP will bind to the modified luciferase, inducing a conformational shift that facilitates the oxidation of D-luciferin to generate measurable luminescence.

3.2.1. Functional Allostery and Dose-Response Profile

To begin, functional allostery was examined using dopamine (DA) and MLS1082, an established D1R positive allosteric modulator, as a positive control (Figure 3.2).[70] In the presence of dopamine, ASP4345 elicits a functional response between approximately 40-70% of the maximal DA control RLU at concentrations 3 to 4-fold lower than required for the DA + MLS1082 samples in both species. At similarly low concentrations, MLS1082 only produces effects between around 7-12% of the maximal control response in hD1R and appears largely ineffective at rD1R. These preliminary results suggest that ASP4345 may exhibit intrinsic agonist activity.

Consequently, the experiment was repeated with varying dilutions of 100 μM ASP4345 without dopamine to better characterize the agonism (Figure 3.3). In hD1R and rD1R, the EC50 values were approximately 25 μM and 10 μM, respectively. Compared to the dopamine EC50 values of 7 nM and 5 nM (see Figure 3.2), ASP4345 is 4-fold less potent, indicating weak agonism.

To clarify the dose-response profile of ASP4345 and dopamine, several concentration ranges of the former were prepared to span between 0.1-100 μM (Figure 3.4). In both species, ASP4345 continued to reinforce initial functional responses at concentrations 2 to 4-fold lower than the control. Nevertheless, in rD1R, the highest 100 μM ASP4345 dose shifted the DA + DMSO EC50 from 2 nM to 0.2 nM, whereas in hD1R, the value shifted from 25 nM to 24 nM; this signifies single-fold and negligible changes in the rat and human receptors, respectively. Additionally, the 100 μM ASP4345 dose generated maximal RLUs between 100-110%, delineating the 'ceiling' of dopaminergic potentiation.

Overall D1-class activity was explored by expressing the structurally homologous rat D5R (rD5R) and comparing ASP4345 functional responses between the two D1-class receptors (Figure

3.5). For rD1R and rD5R, the ASP4345 curves demonstrate similar EC50 values of 2.7 μM and 1.3 μM, respectively; this signifies that the low potency of ASP4345 is analogous between these receptors. As a whole, these experiments imply that ASP4345 exhibits allosteric binding, maintains weak agonism, and stimulates activity at both D1-class receptors.

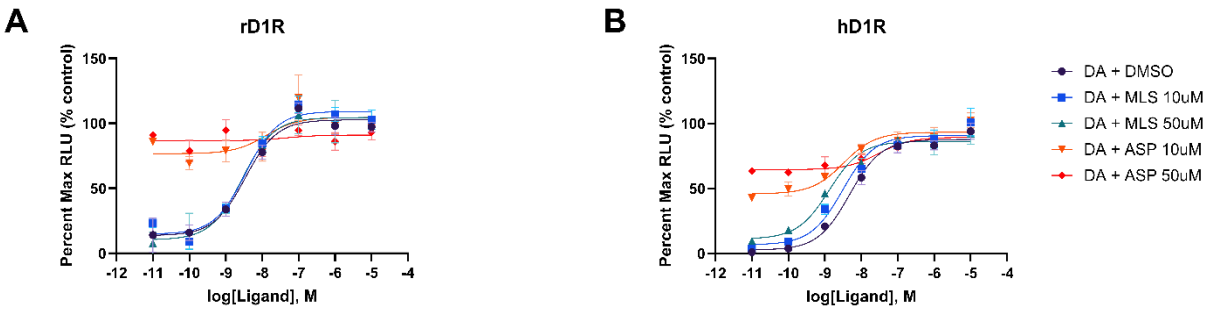

Figure 3.2. Evaluation of ASP4345 as a Positive Allosteric Modulator. D1R expressed in HEK293T-Glo cells treated with DA and varying concentrations of MLS1082 and ASP4345. **(A)** rD1R Best-fit EC50: DA + DMSO = 3.5 nM **(B)** hD1R Best-fit EC50: DA + DMSO = 4.8 nM. The results were plotted as a percentage of maximal RLU normalized to the dopamine control (DA + DMSO), with mean ± SEM of triplicate luminescence measurements for each data point. Curves of best fit were calculated based according to the log(agonist) vs. response (three parameters) function on GraphPad Prism 10.

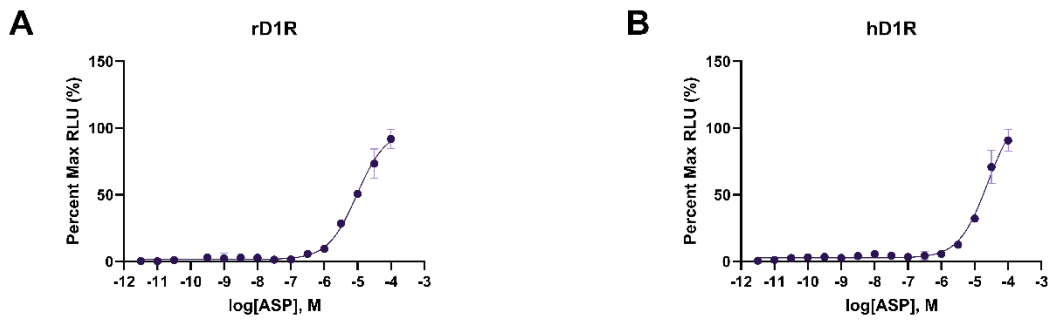

Figure 3.3. Characterization of ASP4345 Agonist Activity. D1R expressed in HEK293T-Glo cells treated with cells treated with 100 μM ASP4345. **(A)** rD1R Best-fit EC50 = 10 μM **(B)** hD1R Best-fit EC50 = 25 μM. The results were plotted as a percentage of maximal RLU, with mean ± SEM of triplicate luminescence measurements for each data point. Curves of best fit were calculated based according to the log(agonist) vs. response (three parameters) function on GraphPad Prism 10.

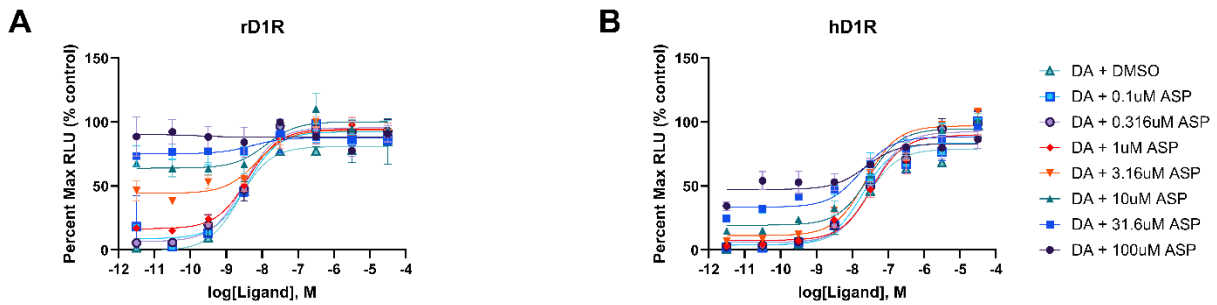

Figure 3.4. Analysis of ASP4345 Dose-Response Profile. D1R expressed in HEK293T-Glo cells treated with cells treated with dopamine and 0-100 μM ASP4345. **(A)** rD1R Best-fit EC50: DA + DMSO = 2.3 nM; + 0.1 μM ASP = 3.7 nM; + 0.316 μM ASP = 3.1 nM; + 1 μM ASP = 3.9 nM; + 3.16 μM ASP = 7.2 nM; + 10 μM ASP = 13 nM; + 31.6 μM = 5.1 nM; + 100 μM = 0.17 nM. **(B)** hD1R Best-fit EC50: DA + DMSO = 25 nM; + 0.1 μM ASP = 19 nM; + 0.316 μM ASP = 36 nM; + 1 μM ASP = 36 nM; + 3.16 μM ASP = 24 nM; + 10 μM ASP = 29 nM; + 31.6 μM = 17 nM; + 100 μM = 24 nM. The results were plotted as a percentage of maximal RLU normalized to the dopamine control (DA + DMSO), with mean ± SEM of triplicate luminescence measurements for each data point. Curves of best fit were calculated based according to the log(agonist) vs. response (three parameters) function on GraphPad Prism 10.

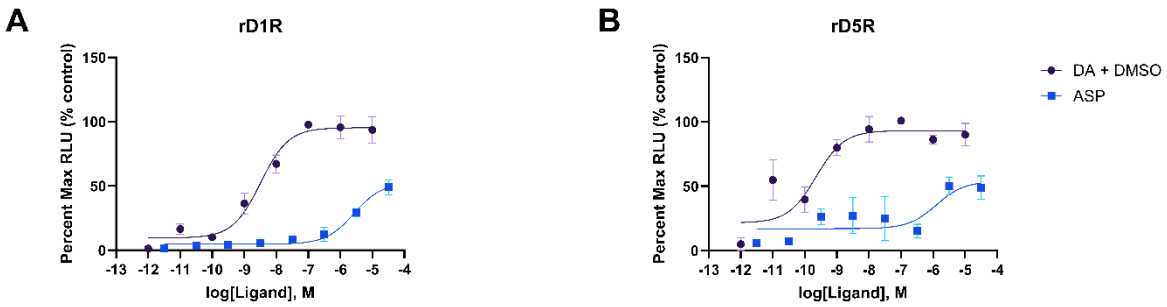

Figure 3.5. Assessment of ASP4345 Activity at D5R. D1R expressed in HEK293T-Glo cells treated with DA and 31.6 µM ASP4345. **(A)** rD1R Best-fit EC50: DA + DMSO = 3.3 nM; 31.6 µM ASP4345 = 2.7 µM **(B)** rD5R Best-fit EC50: DA + DMSO = 0.3 nM; 31.6 µM ASP4345 = 1.3 µM. The results were plotted as a percentage of maximal RLU normalized to the dopamine control (DA + DMSO), with mean ± SEM of triplicate luminescence measurements for each data point. Curves of best fit were calculated based according to the log(agonist) vs. response (three parameters) function on GraphPad Prism 10.

3.3. Radiolabelling Strategy Screening

When ascertaining radiolabelling strategies, identifying applicable precursors and viable radiosynthetic approaches is essential. Accordingly, three approaches were proposed along those lines: [^{11}C]CO_2 fixation, ^{18}F-fluorination, and ^{11}C-methylation.

3.3.1. [^{11}C]CO_2 Fixation Aminophenol Precursor Routes

Given ASP4345 contains an oxazolidinone, an analogous aminophenol precursor was proposed to adopt an established [^{11}C]CO_2 fixation radiolabelling strategy (Figure 3.6).[71] As the reactivity of the exposed phenol was expected to interfere with ensuing reactions in the ASP4345 route, three protecting groups were assessed based on stability and compatibility with subsequent synthetic steps: methyl ether, benzyl ether, and methoxyethoxy methyl ether (Figure 3.7).

For methyl ether, beginning with 5-chloro-2-methoxyaniline as the protected 'building block' for the route, an amine alkylation reaction was performed.[72] However, the remainder of the synthesis was carried out using the same procedures as the original ASP4345 standard, culminating in a yield of 95% in the final step. Although demethylation was attempted using a solution of lithium chloride in dimethylformamide (DMF), the desired aminophenol precursor was not reflected in the ensuing chromatographic analyses. Therefore, additional demethylation strategies were screened in a series of small-scale test reactions by comparing against the commercially available standard, 5-chloro-2-aminophenol, on UPLC-MS.[73–79] As summarized by Table 3.1, the desired product was not detected in any of the sampled mixtures.

Table 3.1: Summary of Demethylation Conditions and Results

Reaction Type	Demethylating Agent(s)	Solvent(s)	UPLC-MS Detection
Nucleophilic	*tert*-butyl thiol	*N*-methyl-2-pyrrolidone	No
Nucleophilic	sodium *N*-methylaniline	xylene, hexamethylphosphoramide	No
Lewis Acid	aluminum chloride	acetonitrile	No
Lewis Acid	aluminum chloride, boron trifluoride diethyl etherate	acetonitrile, chloroform	No
Brønsted Acid	hydrobromic acid	N/A	No
Brønsted Acid	sulfuric acid	N/A	No

After exhausting the methyl ether route, benzyl ether installation and cleavage was evaluated as another protection strategy. Starting with 5-chloro-2-aminophenol, the protection reaction was carried out using benzyl bromide in a basic environment.[80] Although mixture of benzylated products were observed on thin-layer chromatography, the *O*-benzyl fractions were isolated using silica column chromatography. To cleave the benzyl ether, a hydrogenation reaction was performed with palladium on carbon catalyst.[74] Nevertheless, no conversion was observed on TLC, nor did the reaction mixture contain the 5-chloro-2-aminophenol standard according to UPLC-MS.

Lastly, methoxyethoxy methyl ether installation was explored using 5-chloro-2-chlorophenol and 2-methoxyethoxyl methyl chloride and three conditions with varying properties, such as differing bases and a phase-transfer catalyst.[81–83] As detailed in Table 3.2, the desired product was not detected in any of the sampled mixtures by UPLC-MS.

Table 3.2: Summary of Methoxyethoxy methyl ether Installation Conditions and Results

Reactive Property	Key Reagent	Solvent(s)	UPLC-MS Detection
Strong Base	diisopropylethylamine	dichloromethane	No
Strong Base	sodium hydride	tetrahydrofuran	No
Phase-Transfer Catalyst	tetrabutylammonium bromide	sodium hydroxide/ dichloromethane solution	No

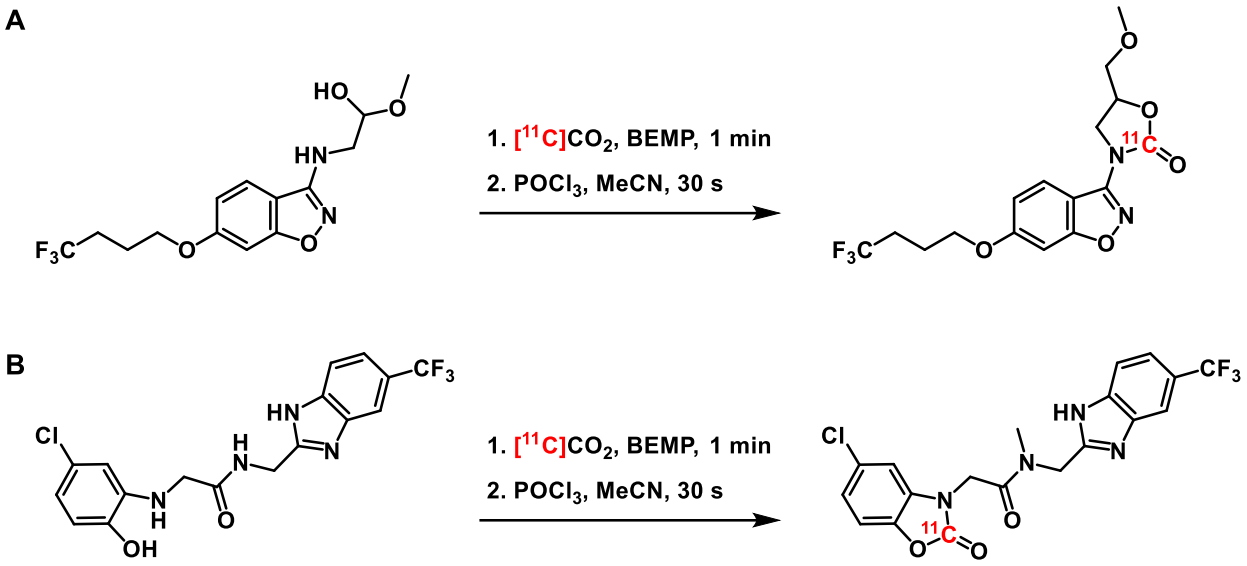

Figure 3.6. Proposed [^{11}C]CO_2 Fixation Radiolabelling Strategy. The applicability of the oxazolidinone radiolabelling site to ASP4345 supported the development of an aminophenol precursor.

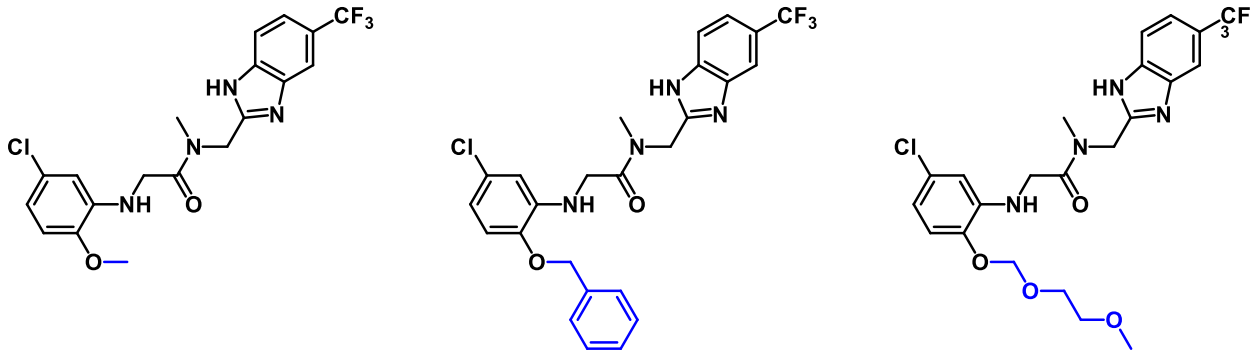

Figure 3.7. Phenol Protection Options for [^{11}C]CO_2 Fixation Precursor. Methyl ether, benzyl ether and methoxyethoxy methyl ether were initially considered to be feasible phenol protection strategies given their compatibility with ASP4345 synthesis.

3.3.2. Cu-mediated ^{18}F-Fluorination

To determine whether heterocyclic ASP4345 impeded radiofluorination, two conditions were run in parallel to represent positive control and screening reactions (Figure 3.8). As such, 4-(4,4,5,5-tetramethyl-1,3,2-dioxaborolan-2-yl) benzonitrile served as the model substrate for ^{18}F-fluorination given the presence of aryl pinacol boronate (Bpin), a common precursor in such radiolabelling contexts. Upon capturing the activity in a potassium carbonate and Kryptofix 222 solution, it was added to a mixture of the catalyst, tetrakis(pyridine)copper (II) triflate, and Bpin substrate in DMF. For the screening reactions, an equimolar amount of ASP4345 was added along with the precursor. After allowing each mixture to stir for 20 minutes at 110 °C, radio-TLC analysis was performed to assess radiochemical yield (RCY). The positive control reactions (n = 2) showed conversion of 20% (± 4%), whereas the ASP4345 screening reactions (n = 2) yielded no detectable product.

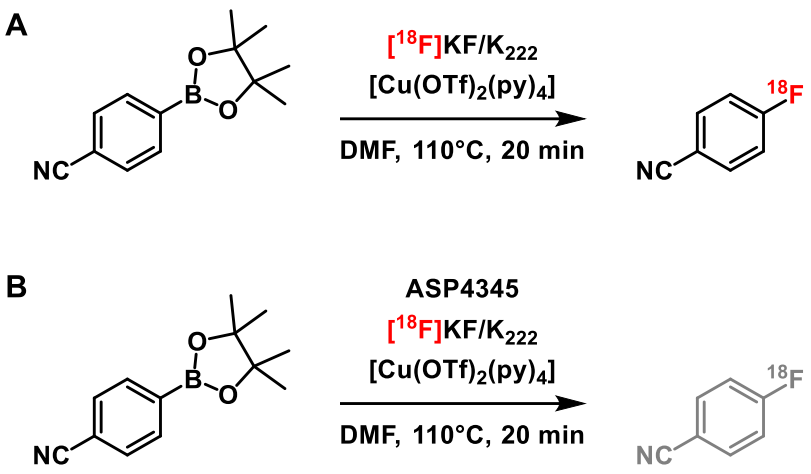

Figure 3.8. Cu-mediated ^{18}F-Fluorination Derisking Experiment. Upon comparing **(A)** positive control reactions (RCY = 20 ± 4%) to **(B)** ASP4345 screening reactions (no discernible product), radiochemical yields suggested that the heterocyclic nature of the tracer candidate adversely affected Cu-mediated ^{18}F-fluorination.

3.3.3. ^{11}C-Methylation Acetamide Model Substrates

To determine the viability of ^{11}C-methylation based on established radiosynthetic methods for [^{11}C]flumazenil, an acetamide standard and precursor were synthesized to model the amide functionality and reactivity of ASP4345 (Figure 3.9).[84] Both the precursor and standard were produced using the appropriate aryl amine substrates along with acetic anhydride in a basic reaction environment (Figure 3.10).[67] In so doing, the *N*-benzylacetamide precursor and *N*-benzyl-*N*-methylacetamide standard were produced in yields of 71% and 67%, respectively. These compounds will enable subsequent ^{11}C-methylation screening experiments, thereby facilitating preliminary assessment of this radiolabelling strategy prior to developing an ASP4345 precursor.

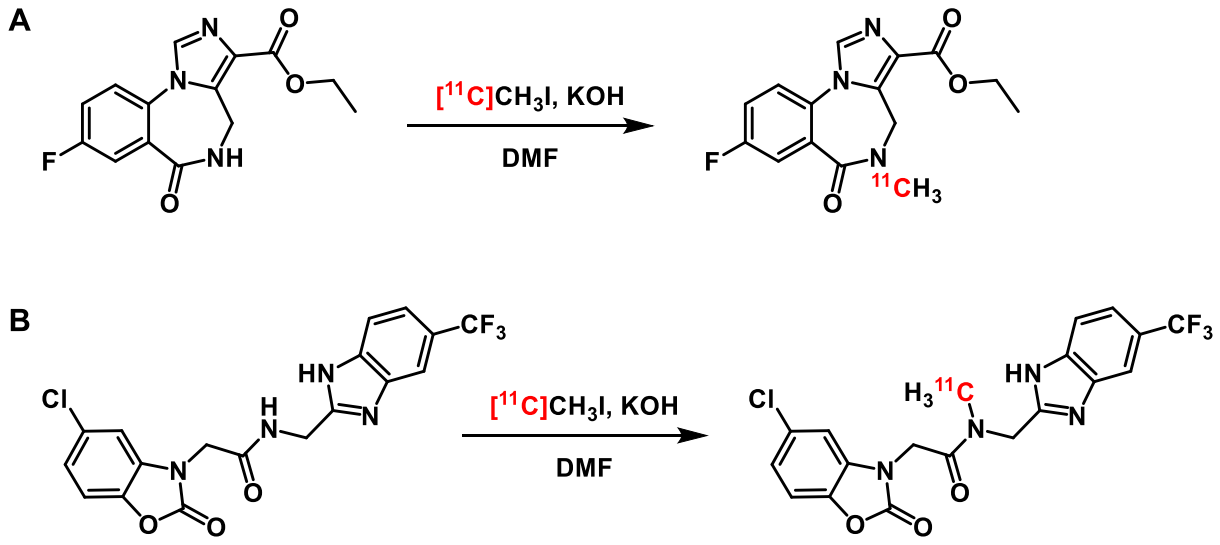

Figure 3.9. Adapting Radiosynthesis of [^{11}C]FMZ to ASP4345. (A) ^{11}C-methylation conditions based on procedures established for [^{11}C]flumazenil involve radiolabelling a secondary amide. **(B)** An ASP4345 precursor could be developed with a secondary amide to enable this radiosynthetic approach.

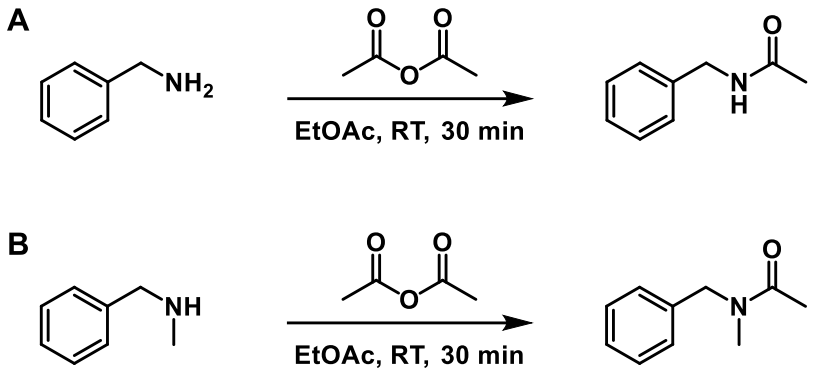

Figure 3.10. Synthesis of Acetamide Model Compounds for ^{11}C-Methylation. Acetylation reactions were performed using **(A)** benzylamine and **(B)** *N*-methylbenzylamine to yield the model precursor *N*-benzylacetamide (71%) and standard *N*-benzyl-*N*-methylacetamide (67%).

CHAPTER IV: DISCUSSION

4.1. *In vitro* Pharmacological Characterization

The rationale behind an allosteric radiotracer lies in the hypothesized selectivity advantage. Allosteric sites are less conserved between receptors, even within subtypes, supporting more target-specific interactions.[62,85,86] Therefore, the primary motivation behind our pharmacological characterization was to affirm whether ASP4345 engaged allosterically with D1R. Given that radiotracer evaluation requires animal studies, ensuring that ASP4345 associated with both rat and human receptors was crucial, especially given the heightened species differences between allosteric sites.[62,85,86] To this effect, the GloSensor assays consistently showed that ASP4345 promoted a functional response without competing with dopamine. Orthosteric binding would manifest in a rightward dose-response shift as the dopamine agonist was displaced by increasing concentrations of ASP4345. Because a leftward shift was observed, the compound likely binds to a non-orthosteric site to potentiate dopamine activity, signifying allosterism.

Using a fluorescence-based cAMP assay and hD1R, the original Astellas Pharma patent describes ASP4345 as a positive allosteric modulator based on two key findings: a leftward shift of the dopamine dose-response curve and absence of intrinsic agonistic activity.[63] While the former was observed throughout our GloSensor experiments, ASP4345 also triggered a functional response without dopamine (Figure 3.2). This apparent discrepancy may be explained by the ASP4345 concentration difference between the Astellas Pharma and GloSensor assays. As shown in Figure 3.3, an ASP4345 concentration of approximately 25 μM was required to induce a discernible cAMP effect, which is 2.5x higher than the maximum 10 μM dose tested by Astellas Pharma. Moreover, analogous cAMP accumulation experiments from Luderman et al. (2018)

indicate that the established PAM MLS1082 reduces the dopamine EC50 by 3-fold at 50 μM.[70] When compared to the minimal leftward EC50 shifts reported in Figure 3.4, ASP4345 poorly modulates dopamine potency at D1R. When taken altogether, these observations denote a weak 'ago-PAM' profile, wherein a ligand shows a mixture of modulatory and agonistic interactions.[85]

Additionally, ASP4345 demonstrates greater potency at the rat receptors, as evinced by more pronounced dose-response plateaus, and by extension, saturation (Figures 3.2 and 3.4). Although such *in vitro* results primarily characterize functional responses, the greater effect of ASP4345 on rD1R may be predictive of increased affinity in rodents. Within biodistribution and imaging contexts, this could translate to a comparatively higher binding potential in preclinical studies. While not inherently problematic, the resulting findings may be less representative of tracer performance and efficacy in humans.

4.2. Radiolabelling Strategy Screening

4.2.1. [^{11}C]CO_2 Fixation Aminophenol Precursor Routes

The initial design and radiolabelling of an aminophenol precursor was based on [^{11}C]CO_2 fixation conditions established by Vasdev et al. (2011).[71] In this procedure, a carbon-11 labelled oxazolidinone is formed from the carbonylation of a secondary amine and adjacent alcohol (Figure 3.6). Because the synthetic context of ASP4345 favoured beginning with an aminophenol, selectivity challenges were anticipated with the phenol during the final coupling step, likely producing a mixture of unwanted products. Thus, various protection strategies were investigated to mitigate such side reactions.

Ether-based protecting groups such as methyl, benzyl, and methoxyethoxy methyl ether offer stability due to their unreactive nature. Both methyl and benzyl ether are stable to acid, which

suggested compatibility with the acidic deprotection in the second synthetic step (see Figure 2.1A). These groups were selected to withstand the entirety of ASP4345 synthesis, after which cleavage would occur to yield the aminophenol precursor. However, this robustness presented the caveat of challenging deprotections, further compounded by identifying conditions that do not interfere with other ASP4345 functionalities. Although a vast array of deprotection reactions was attempted, they failed to demonstrate the desired substrate conversion. The strength of the ether linkage paired with the limited scope of applicable deprotection conditions likely hampered these protection strategies.

Conversely, while methoxyethoxy methyl ether is acid labile, installation was planned after the acidic second synthetic step to avoid premature deprotection. The MEM was then expected to tolerate the amide bond formation before being cleaved in the final hydrochloric acid step. Nonetheless, test reactions to incorporate methoxyethoxy methyl ether failed to yield the desired product. Considering the mechanistic differences between the conditions, deficiencies in the common variable, the MEM-Cl reagent, are probable as suggested by preliminary characterization data. As such, this protection strategy demands re-evaluation following MEM-Cl purification by calcium chloride and fractional distillation.[87]

Given the synthetic challenges associated with producing a [^{11}C]CO_2 fixation aminophenol precursor, additional radiosyntheses were explored using a 'screening' process. In other words, radiolabelling approaches will be identified by approximating ASP4345 reactivity in test reactions. By using an ASP4345 additive or simplified model substrate, radiosynthetic viability is ascertained before precursor development, thereby justifying a chemistry investment.

4.2.2. Cu-mediated ^{18}F-Fluorination

Fluorine-18 is a radioisotope widely incorporated in PET tracers given its lengthy half-life (110 minutes) and the common pharmaceutical application of halogens.[88] In particular, copper-mediated radiofluorination is a popular labelling strategy because readily available [^{18}F]fluoride is employed as a nucleophile, which offers higher specific activity than electrophilic [^{18}F]fluorine.[89] While this reaction is applicable to a variety of substrates, the heterocycles in ASP4345 presented a more complex molecular environment. Consequently, a "derisking" approach delineated by Taylor et al. (2017) determined whether Cu-mediated ^{18}F-fluorination was a feasible strategy before precursor development.[88]

Considering the screening reactions failed to yield radiolabelled products, Chan-Lam coupling between the ASP4345 imidazole and aryl pinacol boronate is suspected (Figure 4.1).[88] This reaction often occurs between amines and aryl boron substrates, with copper catalysts coordinating and deprotonating the former.[90,91] As suspected by Taylor et al. (2017), the shortened distance between the imidazole nitrogen and copper atom is more conducive to coordination, favouring coupling between ASP4345 and the Bpin model substrate rather than forming the ^{18}F-C bond.[88] To address this hypothesis, future experiments could evaluate both heterocyclic fragments of ASP4345 in separate screening reactions, thereby validating whether the imidazole is responsible. Nevertheless, copper-mediated ^{18}F-fluorination appears incompatible with ASP4345, implying that alternative radiolabelling strategies warrant investigation.

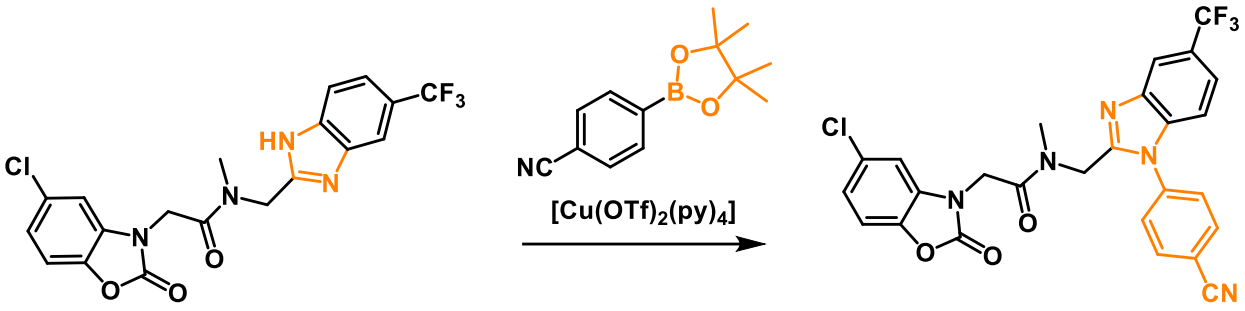

Figure 4.1. Hypothesized Chan-Lam Coupling Reaction. The theoretical distance between the ASP4345 imidazole and copper catalyst is suspected to have created a favourable environment for Chan-Lam coupling with the Bpin substrate, preventing the ^{18}F-fluorination reaction.

4.2.3. ^{11}C-Methylation

^{11}C-methylation is another radiolabelling approach that affixes the carbon-11 radionuclide to heteroatoms via [^{11}C]methyl iodide ([^{11}C]CH_3I). When produced in a gas phase, [^{11}C]CH_3I is formed from the iodination of cyclotron-generated [^{11}C]methane.[92] The highly reactive [^{11}C]methyl iodide enables nucleophilic substitution with a wide range of functionalities, proving highly versatile in radiotracer production.[93] Notably, the radiosynthesis of GABA tracer [^{11}C]flumazenil ([^{11}C]FMZ) uses this reaction to label a secondary amide, a plausible precursor template for ASP4345 (Figure 3.9). To assess the applicability of ^{11}C-methylation, simplified acetamide compounds were synthesized to approximate the reactivity of ASP4345. As such, the model precursor, *N*-benzylacetamide, contains an aromatic ring to resemble similarly electron-withdrawing functionalities on ASP4345. In the future, this substrate will facilitate preliminary assessment of ^{11}C-methylation before synthesizing an ASP4345 precursor.

CHAPTER V: CONCLUSION

5.1. Summary

The dopaminergic system is responsible for a wealth of behavioural functions, namely movement, cognition, and mood. These phenomena are actualized by the mesocorticolimbic and nigrostriatal pathways projecting to the prefrontal cortex and striatum, respectively. Functional abnormalities within these circuits have long been associated with prevalent neurological conditions, ranging from Parkinson's disease to schizophrenia. On a biochemical level, cellular signalling within these neural networks occurs through dopaminergic GPCRs, the most widespread of which is the dopamine D1 receptor. Despite such significant presence and pathophysiological potential, this receptor remains an underexplored facet of the dopaminergic system.

D1R has been studied using positron emission tomography because the modality captures receptor distribution in living organisms. To this effect, benzazepine radiotracers [^{11}C]SCH23390 and [^{11}C]NNC112 have been used to interrogate D1R density in clinical contexts, notably Parkinson's disease and schizophrenia. Although these investigations reveal some regional binding differences relative to disease progression, treatment and healthy controls, the results are inconsistent between studies, and occasionally contradictory. A plausible factor is appreciable off-target binding that misrepresents the signal associated with D1R, potentially inflating reported receptor density. Therefore, a more selective radioligand is required to more accurately elucidate D1R distribution in the living brain.

To address this gap, the suspected positive allosteric modulator ASP4345 was evaluated as a tracer candidate based on a D1R-selective targeting paradigm. Following synthesis and molecular characterization, ASP4345 was assessed in luminescence-based functional assays to

validate its pharmacological profile. Experimental observations revealed allosteric binding paired with agonist and modulatory activity, classifying the compound as an ago-PAM. Next, radiolabelling strategies were explored based on precursor accessibility and radiosynthetic compatibility, with [^{11}C]CO_2 fixation, ^{18}F-fluorination, and ^{11}C-methylation being the chosen approaches. Although [^{11}C]CO_2 fixation and ^{18}F-fluorination appear unfeasible for ASP4345, future experiments will determine whether ^{11}C-methylation is applicable before formulating a precursor.

5.2. Future Directions

The radiotracer evaluation workflow appraises candidates based on physicochemical properties, *in vitro* pharmacology, and biodistribution.[94] Traditionally, such an iterative process depends heavily upon radioligand development, with this key step facilitating binding studies. Such experiments require the radiotracer to perform autoradiography and preclinical PET imaging, both of which provide valuable insight into tissue uptake and distribution. Therefore, conventional tracer evaluation is limited by the synthetic accessibility of a precursor and radioligand alike; this demands a substantial chemistry commitment without compelling, higher-order biological rationale.[94–96]

To bypass the requisite radioligand for autoradiography and preclinical imaging, we propose assessing binding potential using multiple reaction monitoring (MRM) mass spectrometry on sectioned brain homogenate. Outlined by Joshi et al. (2014), this *in vivo* approach entails administering the unlabelled tracer candidate to rodents, whereupon compound distribution is assessed by sacrificing the animals at varying timepoints, sectioning the brain regions of interest, and injecting the processed homogenate into a mass spectrometer to extrapolate binding potential from MRM analyses.[95]

5.3. Closing Remarks

As a whole, our project aimed to evaluate ASP4345 as a positive allosteric modulator radiotracer candidate for D1R. This objective is being addressed through a combination of approaches spanning chemistry, pharmacology, and neuroscience. Through the interdisciplinary techniques detailed, we hope to institute a development pipeline for allosteric radiotracers, enabling efficient evaluation and optimization. In so doing, we enhance the breadth of tools at our disposal to better characterize neurological disease, and by extension, the living brain.

REFERENCES

1. Merino, P. The dopaminergic system. in *Chemical Biology of Neurodegeneration*, 1–39 (Wiley-VCH, 2019).
2. Sun, B. *et al.* Crystal structure of dopamine D1 receptor in complex with G protein and a non-catechol agonist. *Nat. Commun.* **12**, 3305 - 3314 (2021).
3. Jones-Tabah, J., Mohammad, H., Paulus, E. G., Clarke, P. B. S. & Hébert, T. E. The signaling and pharmacology of the dopamine D1 receptor. *Front. Cell. Neurosci.* **15**, 1-28 (2022).
4. Vallone, D., Picetti, R. & Borrelli, E. Structure and function of dopamine receptors. *Neurosci. Biobehav. Rev.* **24**, 125–132 (2000).
5. McCutcheon, R. A., Krystal, J. H. & Howes, O. D. Dopamine and glutamate in schizophrenia: Biology, symptoms and treatment. *World Psychiatry* **19**, 15–33 (2020).
6. Huang, D. *et al.* Dynamic changes in the nigrostriatal pathway in the MPTP mouse model of Parkinson's disease. *Parkinsons Dis.* **2017**, 1-7 (2017).
7. Zaragozá, R. Transport of Amino Acids Across the Blood-Brain Barrier. *Front. Physiol.* **11**, 1-11 (2020).
8. Fernstrom, J. D. & Fernstrom, M. H. Tyrosine, phenylalanine, and catecholamine synthesis and function in the brain. *J. Nutr.* **137**, 1539-1547 (2007).
9. Cumming, P. The life history of dopamine. in *Imaging Dopamine*, 5–18 (Cambridge University Press, 2009).
10. Demchyshyn, L. L., O'Dowd, B. F. & George, S. R. Structure of mammalian D1 and D5 dopamine receptors and their function and regulation in cells. in *Dopamine Receptors and Transporters: Function, Imaging and Clinical Implication* (eds. Sidhu, A., Laruelle, M. & Vernier, P.) 43-70 (CRC Press, 2003).
11. Maziarz, M. *et al.* Revealing the activity of trimeric G-proteins in live cells with a versatile biosensor design. *Cell* **182**, 770-785 (2020).
12. Romanelli, R. J., Williams, J. T. & Neve, K. A. Dopamine receptor signaling: Intracellular pathways to behavior. in *The Dopamine Receptors* (ed. Neve, K. A.) 137–173 (Humana Press, 2010).

13. Missale, C., Nash, S. R., Robinson, S. W., Jaber, M. & Caron, M. G. Dopamine receptors: From structure to function. *Physiol. Rev.* **78**, 189–225 (1998).
14. Wamsley, J. K., Alburges, M. E., McQuade, R. D. & Hunt, M. CNS distribution of D1 receptors: Use of a new specific D1 receptor antagonist, [3H]SCH39166. *Neurochem. Int.* **20**, 123 – 128 (1992).
15. Mansour, A. *et al.* Localization of dopamine D2 receptor mRNA and D1 and D2 receptor binding in the rat brain and pituitary: An in situ hybridization- receptor autoradiographic analysis. *J. Neurosci.* **10**, 2587–2600 (1990).
16. Ford, C. P. The role of D2-autoreceptors in regulating dopamine neuron activity and transmission. *Neurosci. J.* **282**, 13–22 (2014).
17. Hall, H. *et al.* Distribution of D1- and D2-dopamine receptors, and dopamine and its metabolites in the human brain. *Neuropsychopharmacol.* **11**, 245–256 (1994).
18. Goldman-Rakic, P. S. The relevance of the dopamine-D1 Receptor in the cognitive symptoms of schizophrenia. *Neuropsychopharmacol.* **21**, 170–180 (1999).
19. Abi-Dargham, A. *et al.* Dopamine D1R receptor stimulation as a mechanistic pro-cognitive target for schizophrenia. *Schizophr. Bull.* **48**, 199–210 (2022).
20. Martel, J. C. & Gatti McArthur, S. Dopamine receptor subtypes, physiology and pharmacology: New ligands and concepts in schizophrenia. *Front. Pharmacol.* **11**, 1-17 (2020).
21. Seamans, J. K. & Robbins, T. W. Dopamine modulation of the prefrontal cortex and cognitive function. in *The Dopamine Receptors* (ed. Neve, K. A.) 373–398 (Humana Press, 2010).
22. Durstewitz, D. & Seamans, J. K. The computational role of dopamine D1 receptors in working memory. *Int. J. Neural Netw.* **15**, 561–572 (2002).
23. Gagnon, D. *et al.* Striatal neurons expressing D1 and D2 receptors are morphologically distinct and differently affected by dopamine denervation in mice. *Sci. Rep.* **7**, 1-16 (2017).
24. Lahiri, A. K. & Bevan, M. D. Dopaminergic transmission rapidly and persistently enhances excitability of D1 Receptor-expressing striatal projection neurons. *Neuron* **106**, 277-290 (2020).

25. Ginovart, N. & Kapur, S. Dopamine receptors and the treatment of schizophrenia. in *The Dopamine Receptors* (ed. Neve, K. A.) 431–477 (Humana Press, 2010).
26. Gurevich, E. V. & Gurevich, V. V. Dopamine receptors and the treatment of Parkinson's disease. in *The Dopamine Receptors* (ed. Neve, K. A.) 525–584 (Humana Press, 2010).
27. Glatt, S. J., Faraone, S. V. & Tsuang, M. T. How common is schizophrenia? in *Schizophrenia* (eds. Glatt, S. J., Faraone, S. V. & Tsuang, M. T.) 27-34 (Oxford University Press, 2019).
28. Meltzer, H. Y. & Stahl, S. M. The dopamine hypothesis of schizophrenia: A review. *Schizophr. Bull.* **2**, 19–76 (1976).
29. Williams, G. V. & Goldman-Rakic, P. S. Modulation of memory fields by dopamine Dl receptors in prefrontal cortex. *Nature* **376**, 572–575 (1995).
30. Sawaguchi, T. & Goldman-Rakic, P. S. The role of D1-dopamine receptor in working memory: local injections of dopamine antagonists into the prefrontal cortex of rhesus monkeys performing an oculomotor delayed-response task. *J. Neurophysiol.* **71**, 515–528 (1994).
31. Arnsten, A., Cai, J., Murphy, B. & Goldman-Rakic, P. Dopamine D1 receptor mechanisms in the cognitive performance of young adult and aged monkeys. *J. Psychopharmacol.* **116**, 143–151 (1994).
32. Arnsten, A. F. T., Wang, M., Paspalas, C. D. & Witkin, J. M. Dopamine's actions in primate prefrontal cortex: Challenges for treating cognitive disorders. *Pharmacol. Rev.* **67**, 681–696 (2015).
33. Abi-Dargham, A. *et al.* Prefrontal dopamine D1 receptors and working memory in schizophrenia. *J. Neurosci.* **22**, 3708–3719 (2002).
34. Aubert, I. *et al.* Increased D1 dopamine receptor signaling in levodopa-induced dyskinesia. *Ann. Neurol.* **57**, 17–26 (2005).
35. Blanchet, P. J. *et al.* Effects of the full dopamine D1 receptor agonist dihydrexidine in Parkinson's disease. *Clin. Neuropharmacol* **21**, 339–343 (1998).
36. Granov, A., Tiutin, L. & Schwarz, T. The physical basis of positron emission tomography. in *Positron Emission Tomography*, 3–24 (Springer, 2013).

37. Veronese, M. *et al.* Measuring specific receptor binding of a PET radioligand in human brain without pharmacological blockade: The genomic plot. *Neuroimage* **130**, 1–12 (2016).
38. Shinotoh, H. *et al.* Dopamine D1 receptors in Parkinson's disease and striatonigral degeneration: A positron emission tomography study. *J. Neuro.l Neurosurg. Psychiatry* **56**, 467-472 (1993).
39. Kosaka, J. *et al.* Decreased binding of [11C]NNC112 and [11C]SCH23390 in patients with chronic schizophrenia. *Life Sci.* **86**, 814–818 (2010).
40. Hirvonen, J. *et al.* Brain dopamine D1 receptors in twins discordant for schizophrenia. *Am. J. Psychiatry* **163**, 1747–1753 (2006).
41. Doudet, D. J., Jivan, S., Ruth, T. J. & Wyatt, R. J. In vivo PET studies of the dopamine D1 receptors in rhesus monkeys with long-term MPTP-induced Parkinsonism. *Synapse* **44**, 111–115 (2002).
42. Karlsson, P., Farde, L., Halldin, C. & Sedvall, G. PET study of D-1 dopamine receptor binding in neuroleptic-naive patients with schizophrenia. *Am. J. Psychiatry* **159**, 761–767 (2002).
43. Slifstein, M. *et al.* [11C]NNC 112 selectivity for dopamine D1 and serotonin 5-HT2A receptors: A PET study in healthy human subjects. *J. Cereb. Blood Flow Metab.* **27**, 1733–1741 (2007).
44. Ekelund, J. *et al.* In vivo DA D1 receptor selectivity of NNC 112 and SCH 23390. *Mol. Imaging Biol.* **9**, 117–125 (2007).
45. Poels, E. M. P., Girgis, R. R., Thompson, J. L., Slifstein, M. & Abi-Dargham, A. In vivo binding of the dopamine-1 receptor PET tracers [11C]NNC112 and [11C]SCH23390: A comparison study in individuals with schizophrenia. *J. Psychopharmacol.* **228**, 167–174 (2013).
46. Turjanski, N., Lees, A. J. & Brooks, D. J. In vivo studies on striatal dopamine D_1 and D_2 site binding in L-dopa-treated Parkinson's disease patients with and without dyskinesias. *J. Neurol.* **49**, 717–723 (1997).
47. Okubo, Y. *et al.* Decreased prefrontal dopamine D1 receptors in schizophrenia revealed by PET. *Nature* **385**, 634–636 (1997).

48. Billard, W., Ruperto, V., Crosby, G., Iorio, L. C. & Barnett, A. Characterization of the binding of 3H-SCH 23390, a selective D-1 receptor antagonist ligand, in rat striatum. *Life Sci.* **35**, 1885–1893 (1984).
49. Ravert, H. T., Wilson, A. A., Dannals, R. F., Wong, D. F. & Wagner, H. N. Radiosynthesis of a selective dopamine D-1 receptor antagonist: R(+)-7-chloro-8-hydroxy-3-[11C]methyl-1-phenyl-2,3,4,5-tetrahydro-1H-3-benzazepine ([11C]SCH 23390). *Int. J. Radiat. Appl. Instrum.* **38**, 305–306 (1987).
50. Halldin, C. *et al.* Preparation of 11C-labelled SCH 23390 for the in vivo study of dopamine D-1 receptors using positron emission tomography. *Int. J. Radiat. Appl. Instrum.* **37**, 1039–1043 (1986).
51. Kaasinen, V., Vahlberg, T., Stoessl, A. J., Strafella, A. P. & Antonini, A. Dopamine receptors in Parkinson's disease: A meta-analysis of imaging studies. *J. Mov Disord.* **36**, 1781–1791 (2021).
52. Halldin, C. *et al.* Carbon-11-NNC 112: a radioligand for PET examination of striatal and neocortical D1-dopamine receptors. *J. Nucl. Med* **39**, 2061–2068 (1998).
53. Andersen, P. H. *et al.* NNC-112, NNC-687 and NNC-756, new selective and highly potent dopamine D1 receptor antagonists. *Eur. J. Pharmacol.* **219**, 45–52 (1992).
54. Abi-Dargham, A. *et al.* Increased prefrontal cortical D1 receptors in drug naïve patients with schizophrenia: a PET study with [11C]NNC112. *J. Psychopharmacol.* **26**, 794–805 (2012).
55. Cropley, V. L. *et al.* Pre- and post-synaptic dopamine imaging and its relation with frontostriatal cognitive function in Parkinson disease: PET studies with [11C]NNC 112 and [18F]FDOPA. *Psychiatry Res. Neuroimaging* **163**, 171–182 (2008).
56. Bischoff, S., Heinrich, M., Sonntag, J. M. & Krauss, J. The D-1 dopamine receptor antagonist SCH 23390 also interacts potently with brain serotonin (5-HT2) receptors. *Eur. J. Pharmacol.* **129**, 367–370 (1986).
57. Catafau, A. M. *et al.* Imaging cortical dopamine D 1 receptors using [11C]NNC112 and ketanserin blockade of the 5-HT 2A receptors. *J. Cereb. Blood Flow Metab.* **30**, 985–993 (2009).

58. Hall, A., Provins, L. & Valade, A. Novel strategies to activate the dopamine D1 receptor: Recent advances in orthosteric agonism and positive allosteric modulation. *J. Med. Chem.* **62**, 128–140 (2019).
59. DaSilva, J. N., Schwartz, R. A., Greenwald, E. R., Lourenco, C. M., Wilson, A. A. & Houle, S. Dopamine D 1 agonist R-[11C]SKF 82957: Synthesis and in vivo characterization in rats. *Nucl. Med. Biol.* **26**, 537-542 (1999).
60. Blanchet, P. J., Grondin, R., Bedard, P. J., Shiosaki, K. & Britton, D. R. Dopamine D1 receptor desensitization profile in MPTP-lesioned primates. *Eur. J. Pharmacol.* **309**, 13–20 (1996).
61. Blanchet, P. J. *et al.* Effects of the full dopamine D1 receptor agonist dihydrexidine in Parkinson's disease. *Clin. Neuropharmacol.* **21**, 339–343 (1998).
62. Lindsley, C. W. *et al.* Practical strategies and concepts in GPCR allosteric modulator discovery: Recent advances with metabotropic glutamate receptors. *Chem. Rev.* **116**, 6707–6741 (2016).
63. Shiraki, R. et al. Heterocyclic acetamide compound (US9708307B2). *USPTO.* 1-28 (2017).
64. Desai, A. *et al.* Pharmacokinetics of ASP4345 from single ascending-dose and multiple ascending-dose phase I studies. *Clin. Pharmacokinet.* **60**, 79–88 (2021).
65. Astellas Pharma Global Development (2018, July 18 - 2019, October 2). A study to assess the safety and efficacy of ASP4345 as add-on treatment for cognitive impairment in subjects with schizophrenia on stable doses of antipsychotic medication. Identifier NCT03557931. https://clinicaltrials.gov/study/NCT03557931?rank=1
66. Li, Y. *et al.* Syntheses and characterization of nimesulide derivatives for dual enzyme inhibitors of both cyclooxygenase-1/2 and 5-lipoxygenase. *Bioorg. Med. Chem.* **19**, 2074–2083 (2011).
67. Zhang, J., Sugisawa, N., Felton, K. C., Fuse, S. & Lapkin, A. A. Multi-objective Bayesian optimisation using q-noisy expected hypervolume improvement (qNEHVI) for the Schotten–Baumann reaction. *React. Chem. Eng.* **9**, 706–712 (2023).
68. Banerjee, A., Hattori, T. & Yamamoto, H. Regio- and stereoselective (SN2) N-, O-, C- and S-alkylation using trialkyl phosphates. *Synthesis* **55**, 315–332 (2023).

69. Kumar, B. A., Kumari, P., Sona, C. & Yadav, P. N. Chapter 2 - GloSensor assay for discovery of GPCR-selective ligands. in *Methods in Cell Biology* (ed. Shukla, A. K.) 27–50 (Academic Press, 2017).
70. Luderman, K. D. *et al.* Identification of positive allosteric modulators of the D 1 dopamine receptor that act at diverse binding sites. *Mol. Pharmacol.* **94**, 1197–1209 (2018).
71. Vasdev, N. *et al.* Radiosynthesis of [11C]SL25.1188 via [11C]CO2 fixation for imaging monoamine oxidase B. *J. Labelled. Comp. Radiopharm.* **54**, 678–680 (2011).
72. Kawatani, M. *et al.* Fluorescence detection of prostate cancer by an activatable fluorescence probe for PSMA carboxypeptidase activity. *J. Am. Chem. Soc.* **141**, 10409–10416 (2019).
73. Chae, J. Practical demethylation of aryl methyl ethers using an odorless thiol reagent. *Arch. Pharm. Res.* **31**, 305–309 (2008).
74. Wuts, Peter G.M. Protection for phenols and catechols. in *Greene's Protective Groups in Organic Synthesis* (ed. Wuts, Peter G.M.) 475-552 (Wiley, 2014).
75. Loubinoux, B., Coudert, G. & Guillaumet, G. Selective Demethylation of aryl methyl ethers. *Synthesis* **1980**, 638–640 (2002).
76. Kawamura, Y., Takatsuki, H., Torii, F. & Horie, T. Studies of the selective O-Alkylation and dealkylation of flavonoids. XVI. Demethylation of 2′-methoxyacetophenones with anhydrous aluminum chloride or bromide in acetonitrile. *Bull. Chem. Soc. Jpn.* **67**, 511–515 (1994).
77. Chapelat, J., Buss, A., Chougnet, A. & Woggon, W. D. Diastereoselective synthesis of α-tocopherol: A new concept for the formation of chromanols. *Org. Lett.* **10**, 5123–5126 (2008).
78. Li, C., Lobkovsky, E. & Porco, J. Total synthesis of (±)-torreyanic acid. *J. Am. Chem. Soc.* **122**, 10484–10485 (2000).
79. Li, G., Patel, D. & Hruby, V. J. An efficient procedure for the demethylation of aryl-methyl ethers in optically pure unusual amino acids. *Tetrahedron Lett.* **34**, 5393–5396 (1993).
80. Brenneman, J. B. *et al.* Heterocyclic carboxylic acids as activators of soluble guanylate cyclase (WO2016/014463A1). *WIPO*, 1-230 (2016).

81. Everhart, E. T. & Craig, J. C. A facile general route to enantiomeric 1-(4-hydroxyphenyl)alkanols, and an improved synthesis of 4-vinylphenol. *J. Am. Chem. Soc., Perkin Trans.* **1,** 1701–1707 (1991).
82. Michelot, D. & Meyer, M. Facile Protection of phenols and hydroxypyridines: Key components of natural products - A new pathway to orellanine. *Nat. Prod. Res.* **17**, 41–46 (2003).
83. Corey, E. J., Gras, J. L., & Ulrich, P. A new general method for protection of the hydroxyl function. *Tetrahedron Lett.* **17**, 809–812 (1976).
84. Canales-Candela, R. *et al.* Synthesis of [11C]flumazenil ([11C]FMZ). in *Radiochemical Syntheses* (eds. Scott, P.J.H. & Hockley, B.G.) 221-231 (Wiley, 2012).
85. Christopoulos, A. Advances in G protein-coupled receptor allostery: From function to structure. *Mol. Pharmacol.* **86**, 463–478 (2014).
86. Gregory, K. J., Sexton, P. M. & Christopoulos, A. Overview of receptor allosterism. *Curr. Protoc. Pharmacol.* **51**, 1.21.1-1.21.34 (2010).
87. Armarego, W. L. F. & Chai, C. L. L. Chapter 4 - Purification of organic chemicals. in *Purification of Laboratory Chemicals (Fifth Edition)* (eds. Armarego, W. L. F. & Chai, C. L. L.) 80–388 (Butterworth-Heinemann, 2003).
88. Taylor, N. J. et al. Derisking the Cu-mediated 18F-fluorination of heterocyclic positron emission tomography radioligands. *J. Am. Chem. Soc.* **139**, 8267–8276 (2017).
89. Jacobson, O., Kiesewetter, D. O. & Chen, X. Fluorine-18 radiochemistry, labeling strategies and synthetic routes. *Bioconjugate Chem.* **26**, 1–18 (2015).
90. Fatykhov, R. F., Chupakhin, O. N., Rusinov, V. L. & Khalymbadzha, I. A. Chapter 5 - Copper catalysis for triazines. in *Copper in N-Heterocyclic Chemistry* (ed. Srivastava, A.) 161–220 (Elsevier, 2021).
91. Chen, J.-Q., Li, J.-H. & Dong, Z.-B. A review on the latest progress of Chan-Lam coupling reaction. *Adv. Synth. Catal.* **362**, 3311–3331 (2020).
92. Kniess, T., Rode, K. & Wuest, F. Practical experiences with the synthesis of [11C]CH3I through gas phase iodination reaction using a TRACERlabFXC synthesis module. *Appl Radiat. Isot.* **66**, 482–488 (2008).

93. Miller, P. W., Kato, K. & Långström, B. Carbon-11, nitrogen-13, and oxygen-15 chemistry. in *The Chemistry of Molecular Imaging* (eds. Long, N. J. & Wong, W.) 79–103 (Wiley, 2014).
94. Barth, V. & Need, A. Identifying novel radiotracers for pet imaging of the brain: Application of LC-MS/MS to tracer identification. *ACS Chem. Neurosci.* **5**, 1148–1153 (2014).
95. Joshi, E. M. *et al.* Efficiency gains in tracer identification for nuclear imaging: Can in vivo LC-MS/MS evaluation of small molecules screen for successful PET tracers? *ACS Chem. Neurosci.* **5**, 1154–1163 (2014).
96. Need, A., Kant, N., Jesudason, C. & Barth, V. Approaches for the discovery of novel positron emission tomography radiotracers for brain imaging. *Clin. Transl. Imaging* **5**, 265–274 (2017).

APPENDIX

NMR Characterization Data

tert-butyl (5-chloro-2-oxo-1,3,benzoxazole-3(2*H*)-yl) acetate

^{1}H NMR (80 MHz, DMSO-d6)

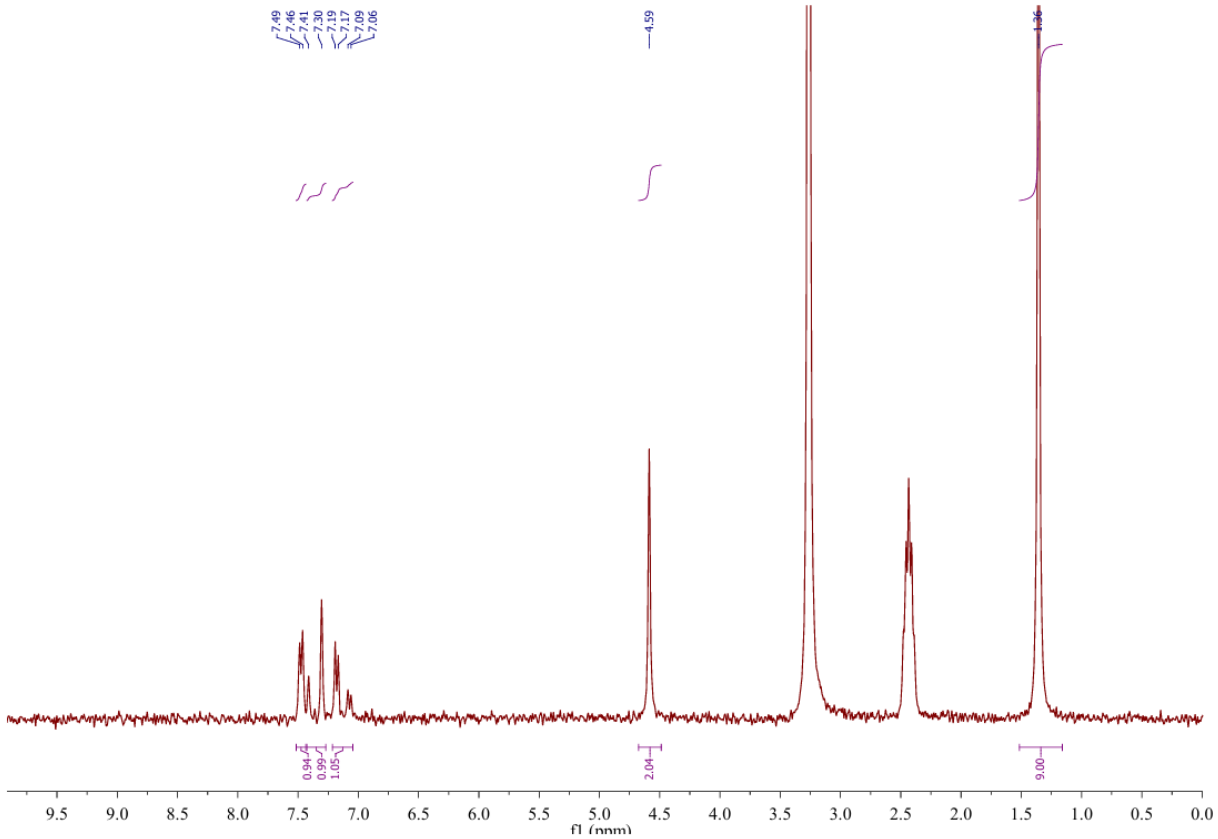

(5-chloro-2-oxo-1,3-benzoxazol-3(2*H*)-yl) acetic acid

^{1}H NMR (80 MHz, DMSO-d6)

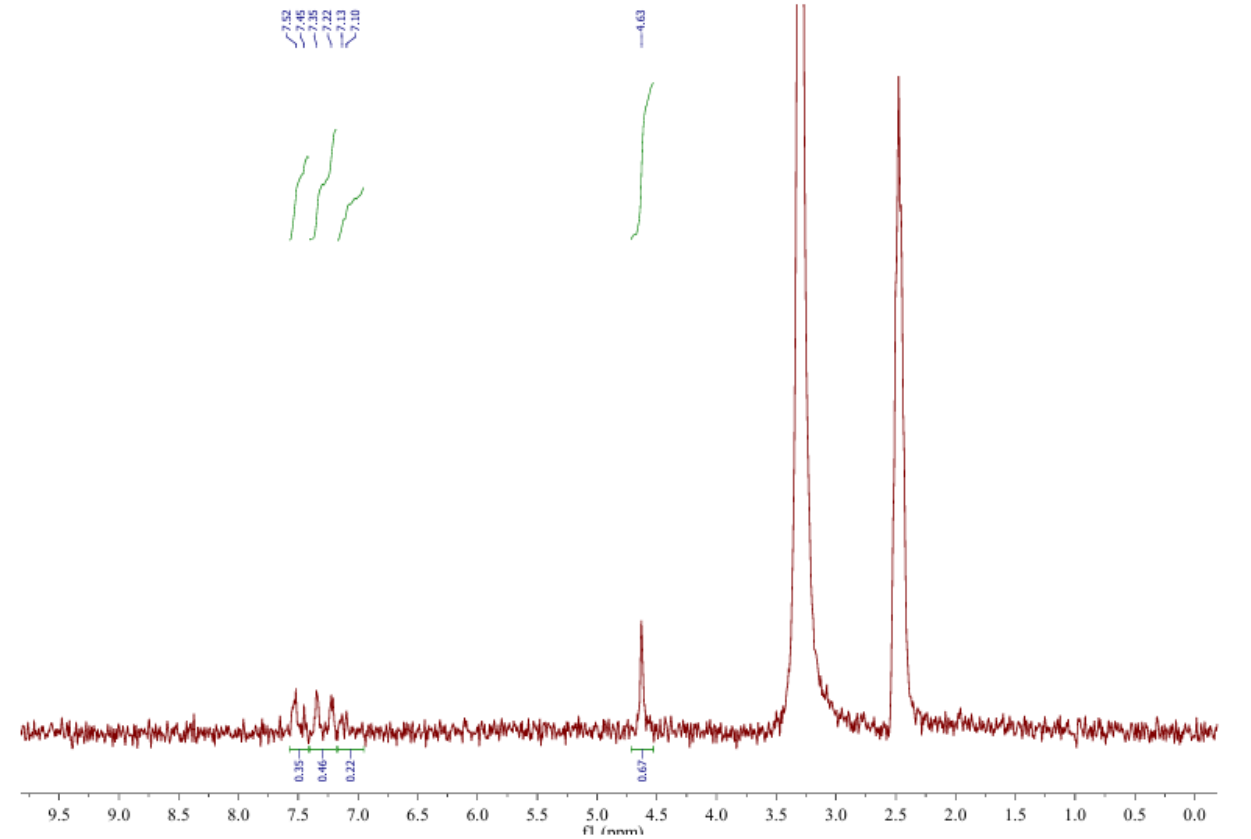

***tert*-butylmethyl{[5-(trifluoromethyl)-1*H*-benzimidazol-2-yl]methyl} carbamate**

^{1}H NMR (80 MHz, $CDCl_3$)

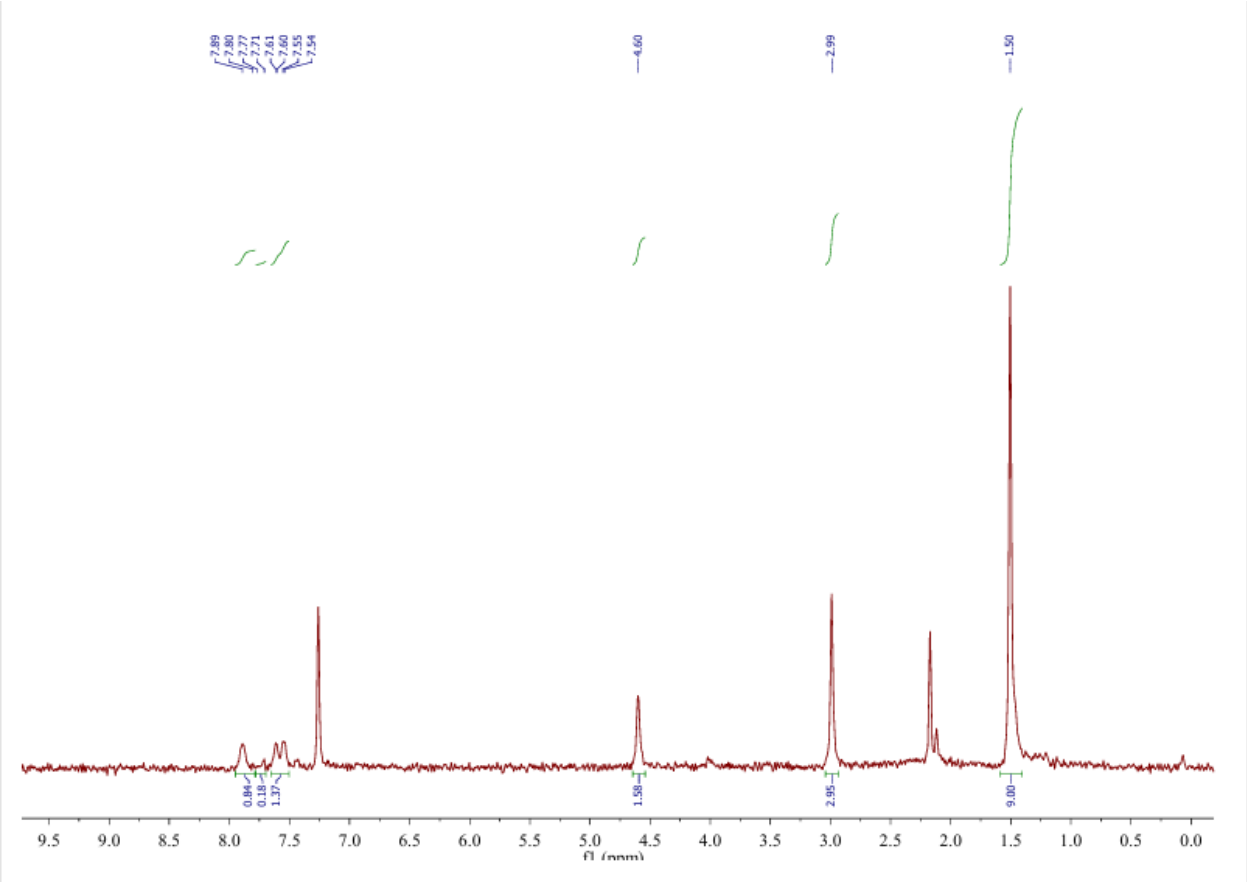

_N_-methyl-1-[5-(trifluoromethyl)-1_H_-benzimidazol-2-yl] methanamine dihydrochloride

^{1}H NMR (80 MHz, DMSO-d6)

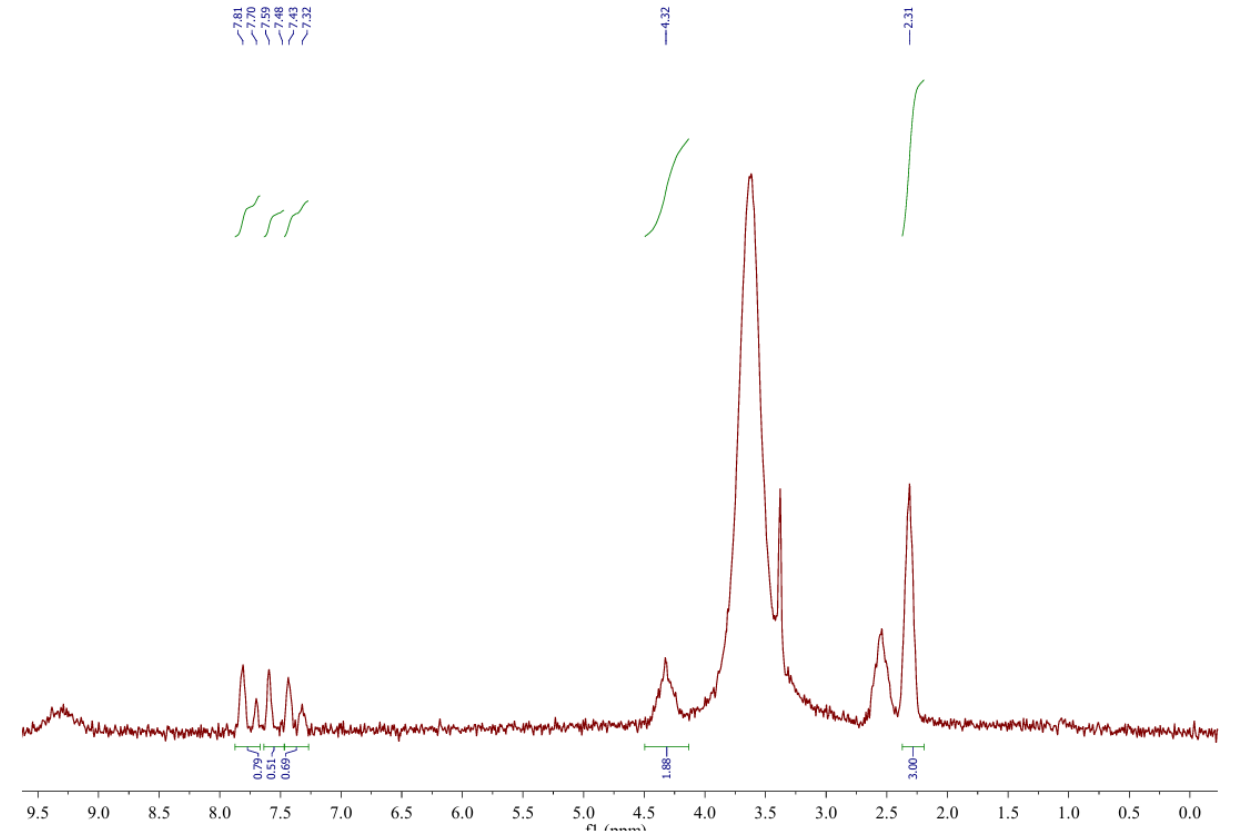

2-(5-chloro-2-oxo-1,3-benzoxazol-3(2*H*)-yl)-*N*-{[5-(trifluoromethyl)-1*H*-benzimidazol-2-yl]methyl} acetamide hydrochloride

^{1}H NMR (400 MHz, DMSO-d6)

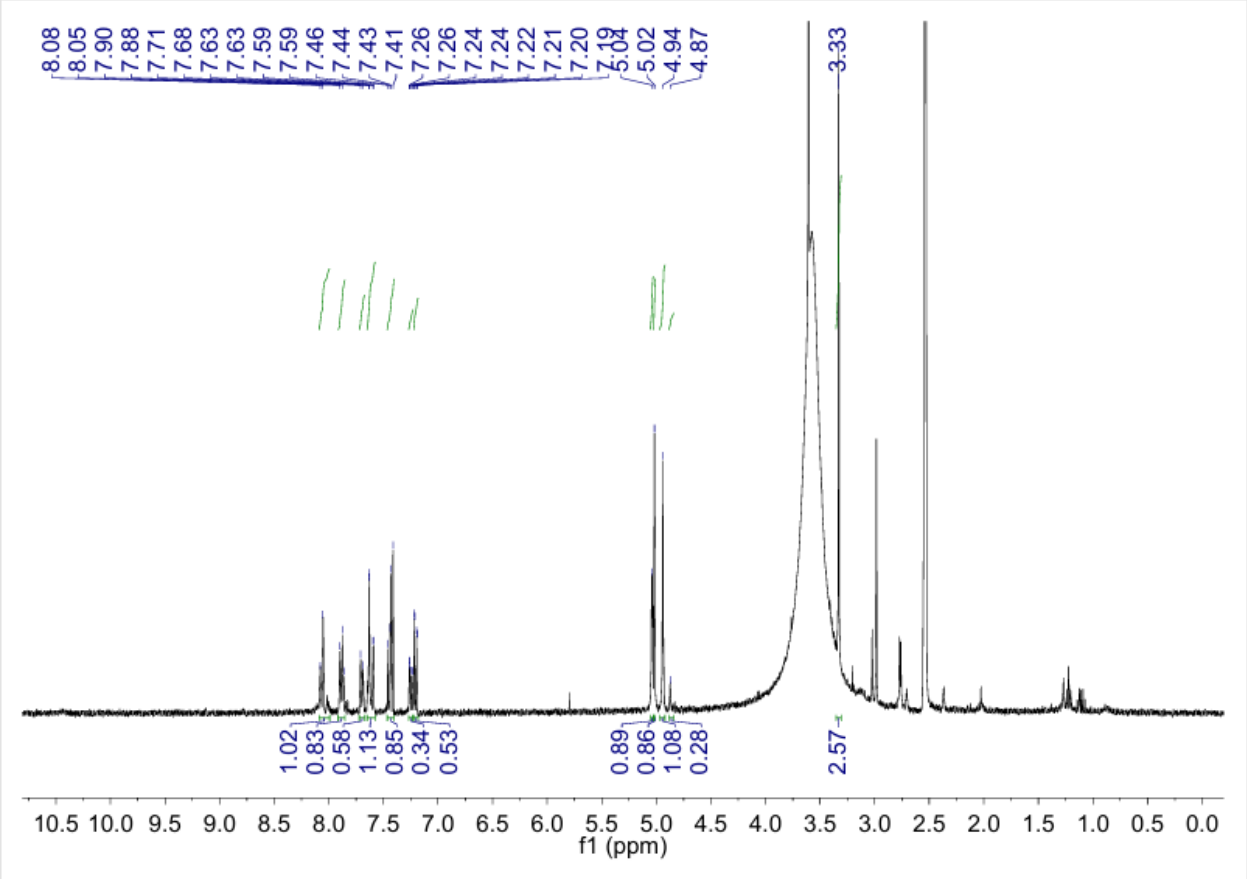

2-methyl-2-propanyl-*N*-(5-chloro-2-methoxyphenyl) glycinate

^{1}H NMR (80 MHz, DMSO-d6)

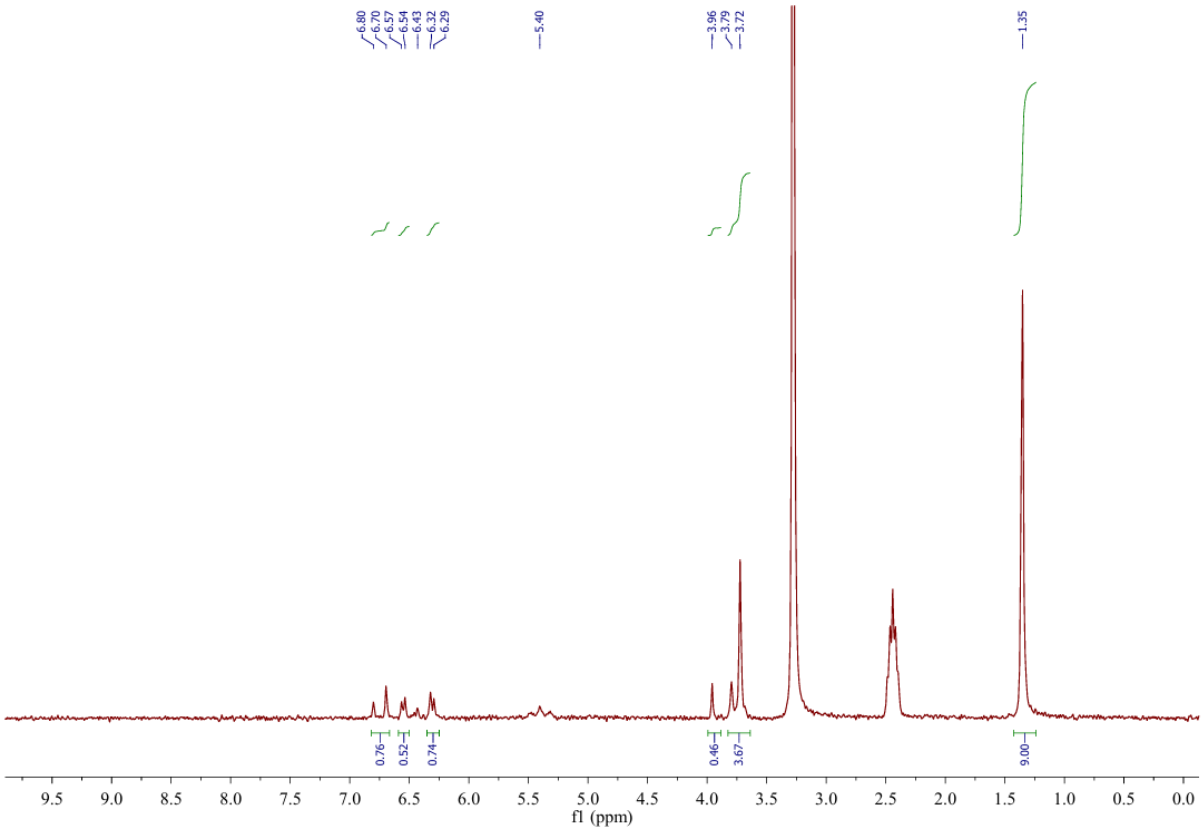

***N*-benzylacetamide**

^{1}H NMR (80 MHz, DMSO-d6)

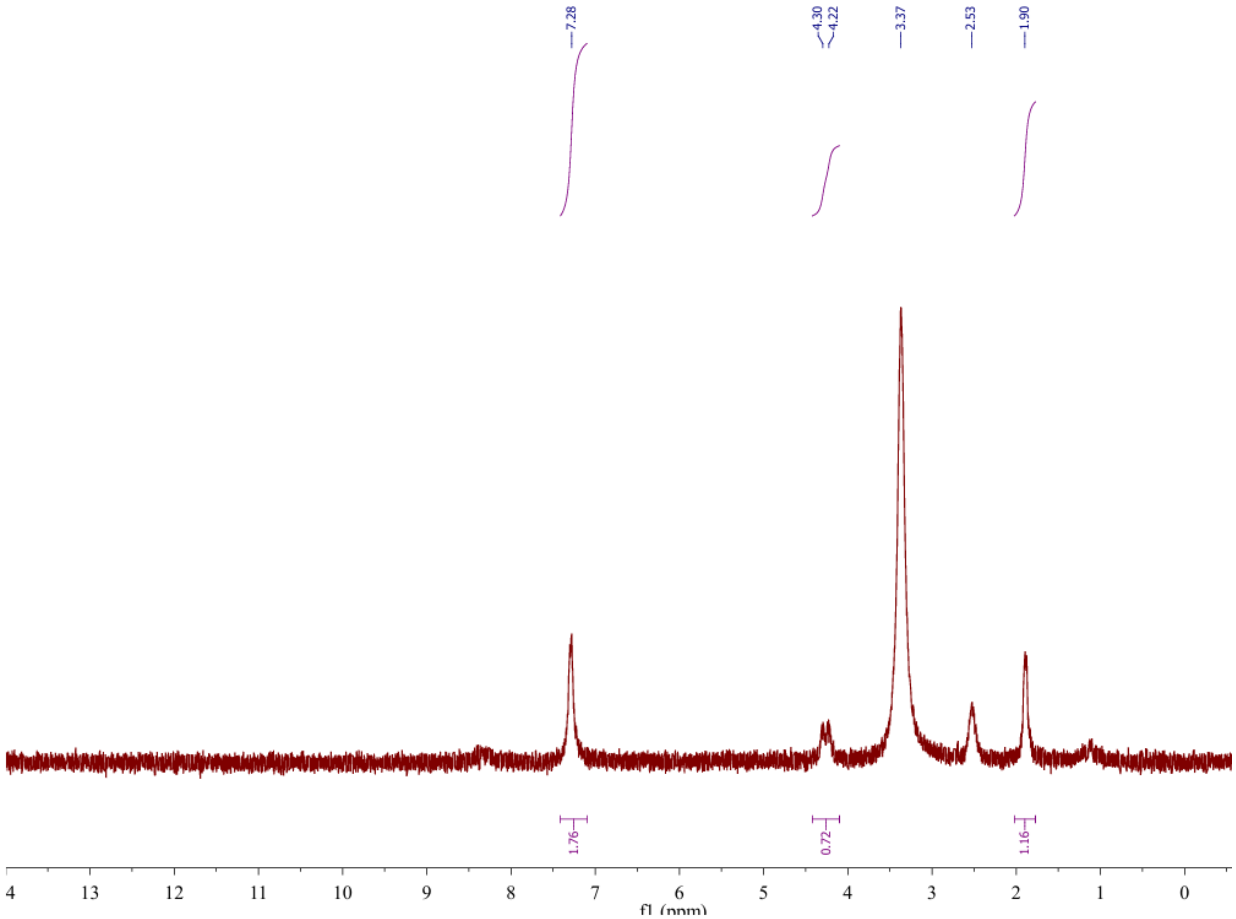

***N*-benzyl-*N*-methylacetamide**

^{1}H NMR (80 MHz, DMSO-d6)

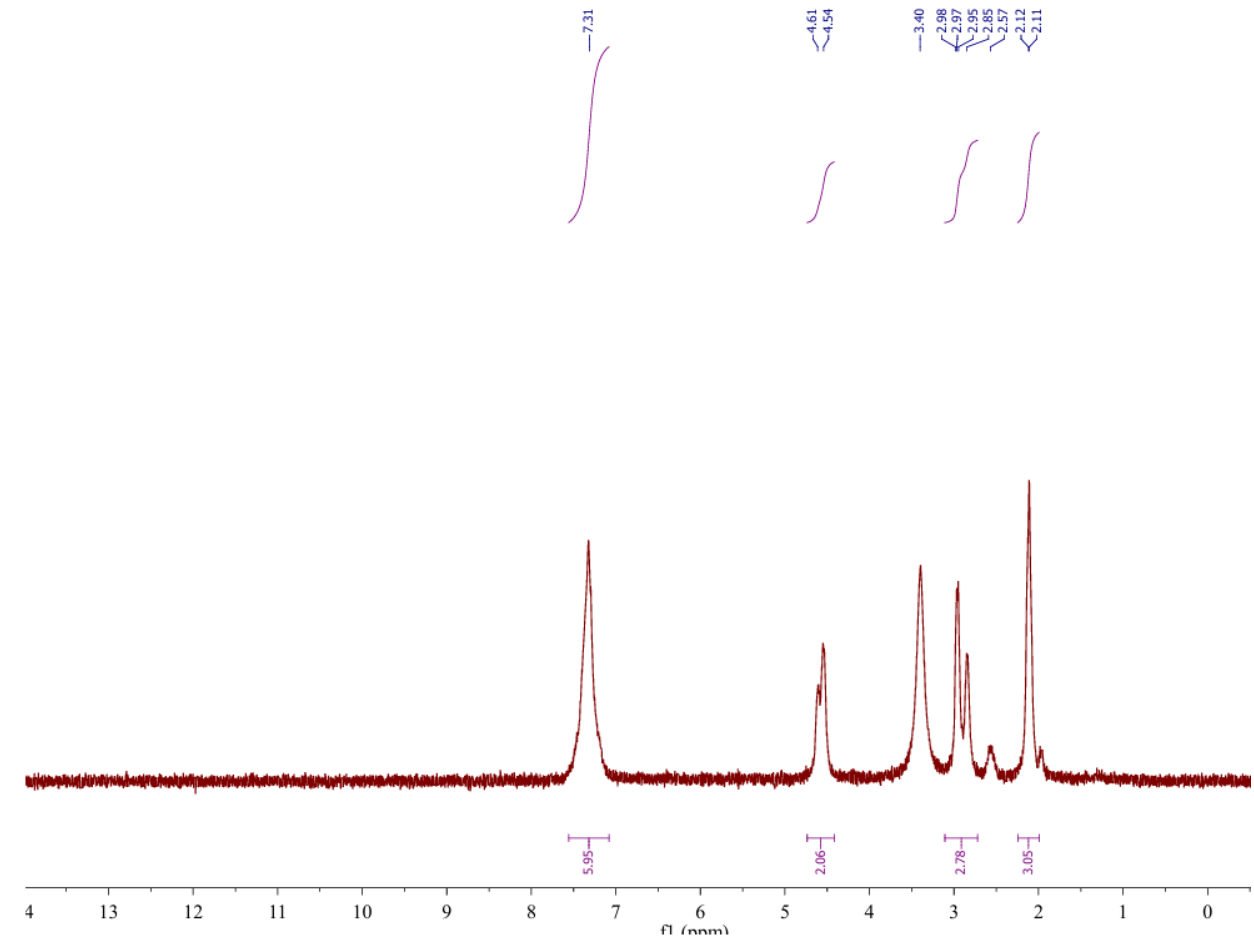

UPLC-MS Characterization Data

2-(5-chloro-2-oxo-1,3-benzoxazol-3(2*H*)-yl)-*N*-{[5-(trifluoromethyl)-1*H*-benzimidazol-2-yl]methyl} acetamide hydrochloride

ESI+

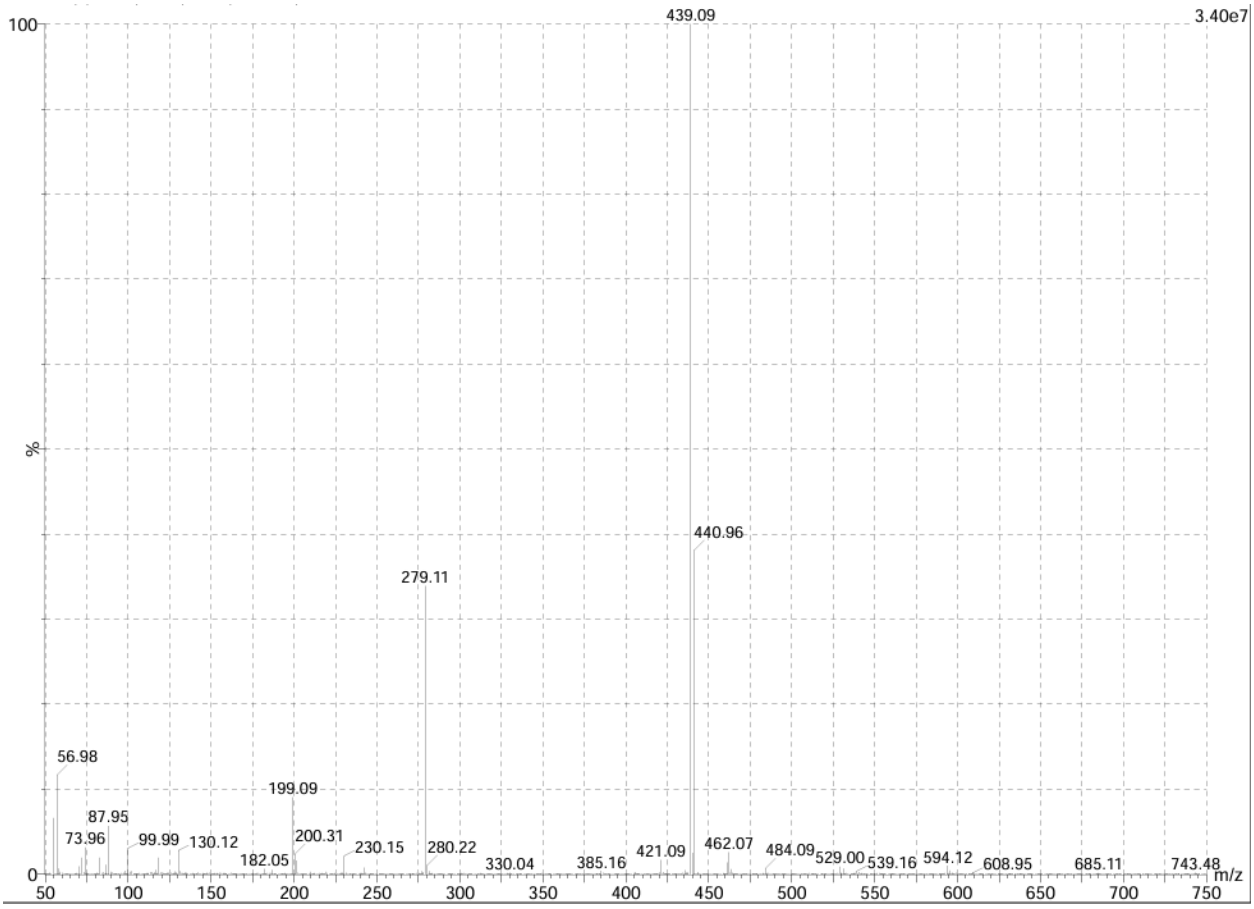

2-methyl-2-propanyl-*N*-(5-chloro-2-methoxyphenyl) glycinate

Diode Array (254 nm)

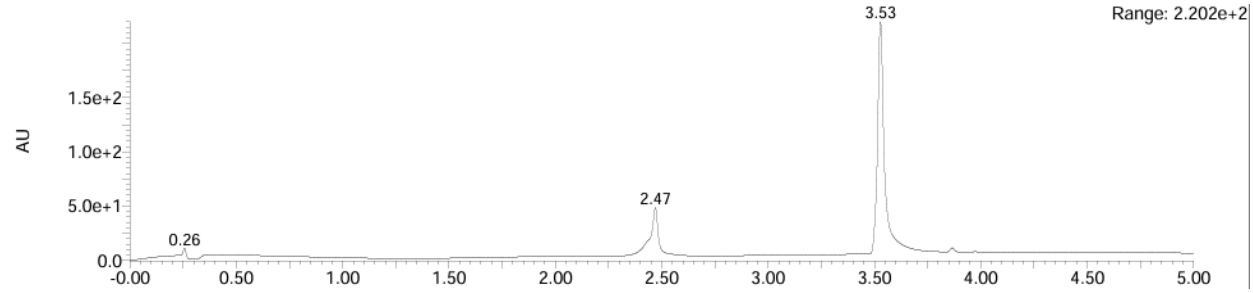

ESI+

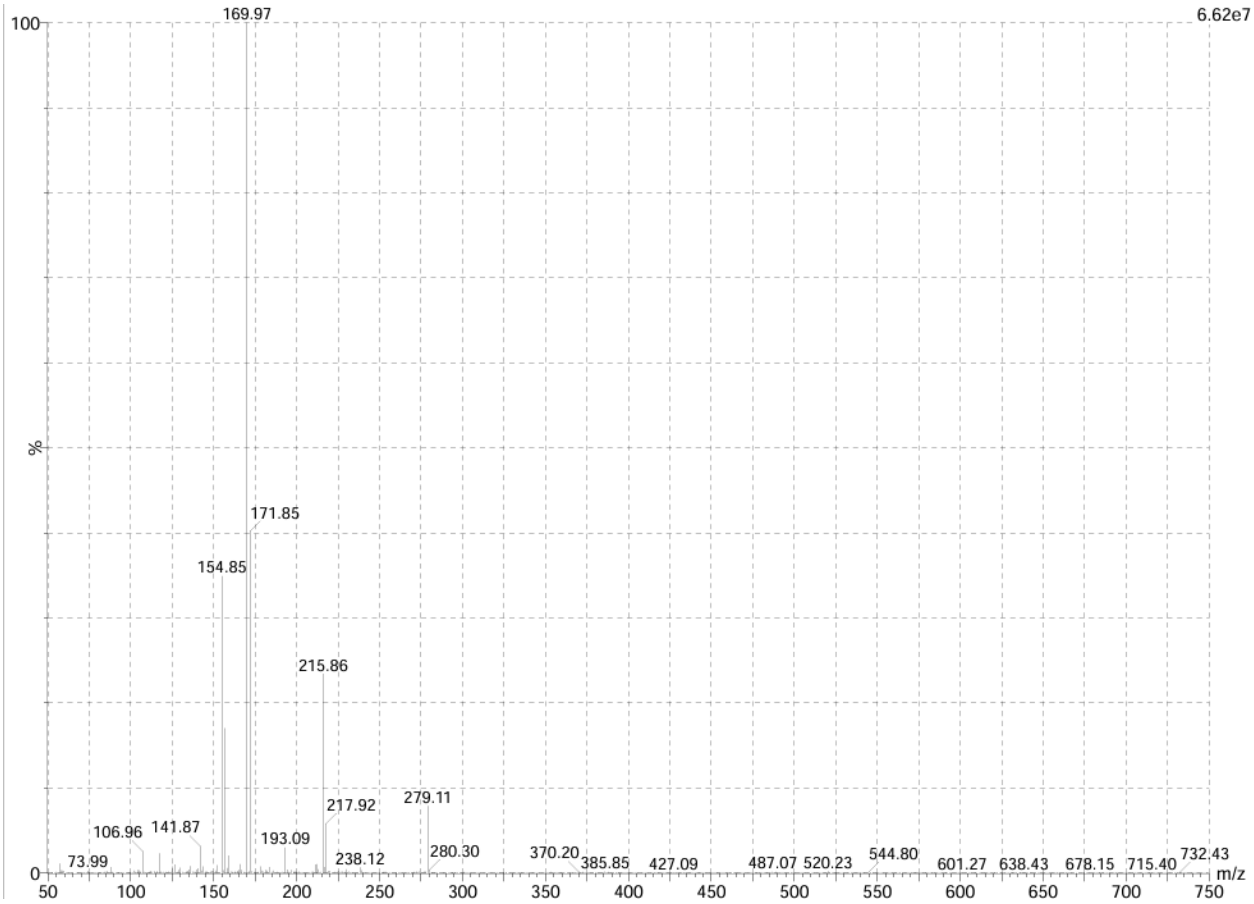

N-(5-chloro-2-methoxyphenyl) glycine

Diode Array (254 nm)

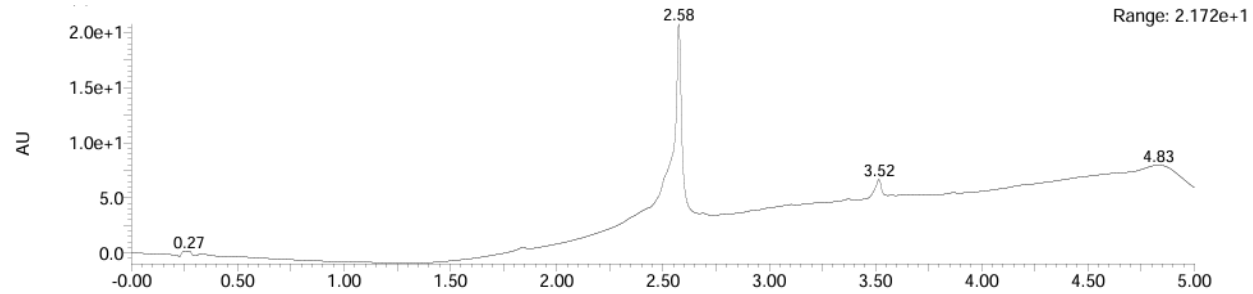

ESI+

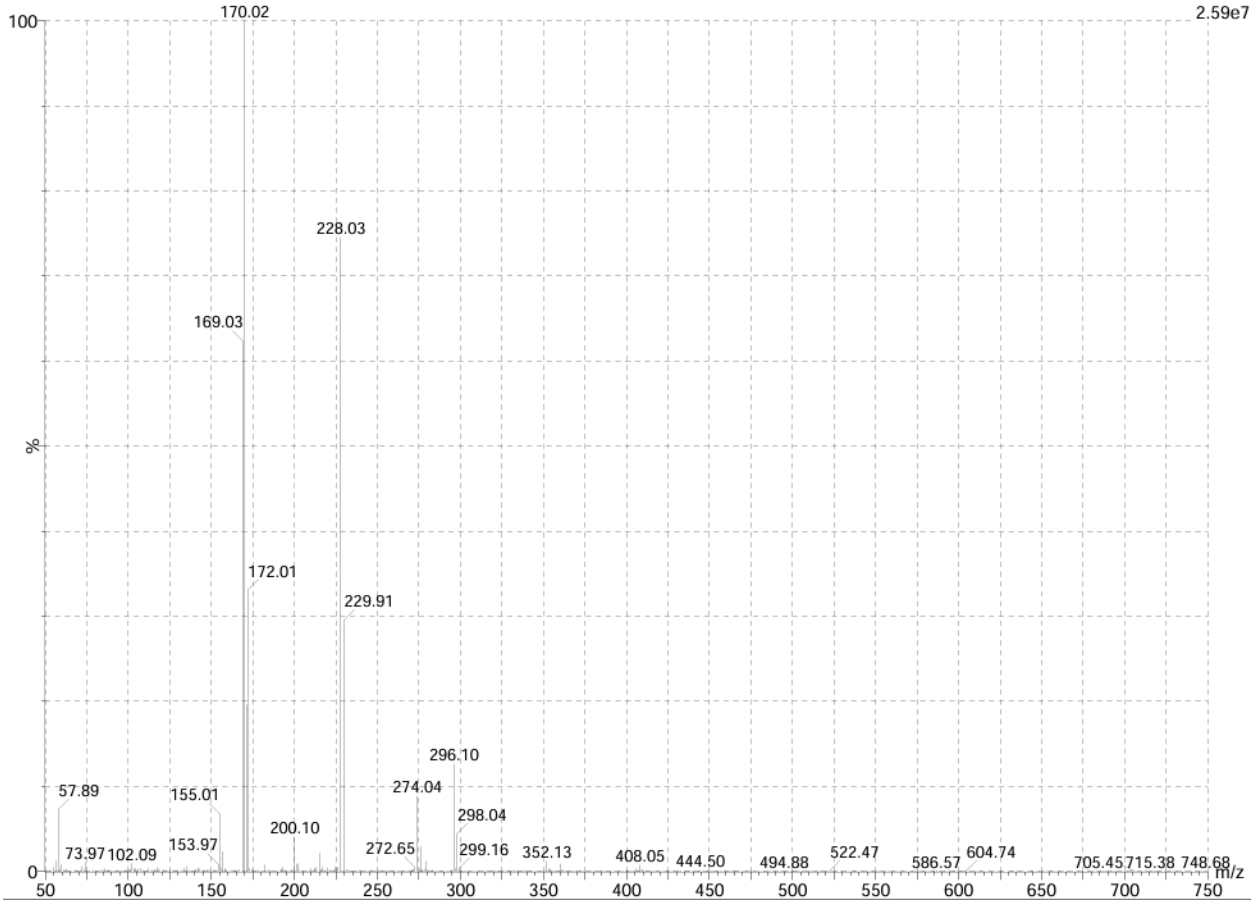

_N_-{[5-(trifluoromethyl)-1_H_-benzimidazol-2-yl]methyl}-2-[(5-chloro-2-methoxyphenyl)amino]-_N_-methylacetamide

Diode Array (254 nm)

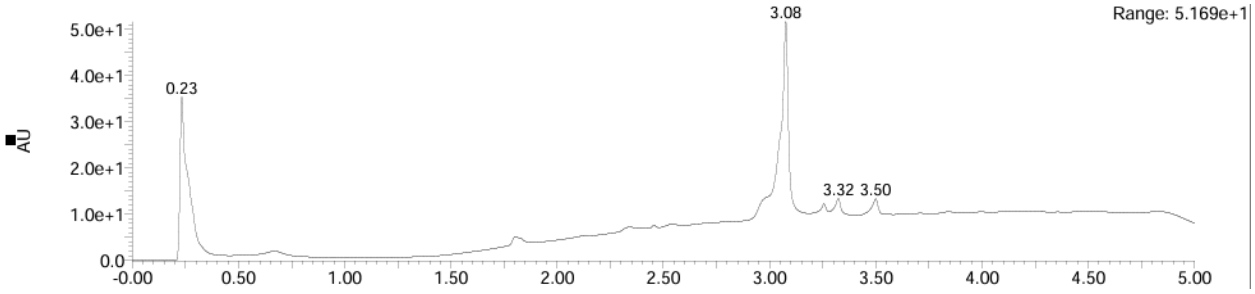

ESI+

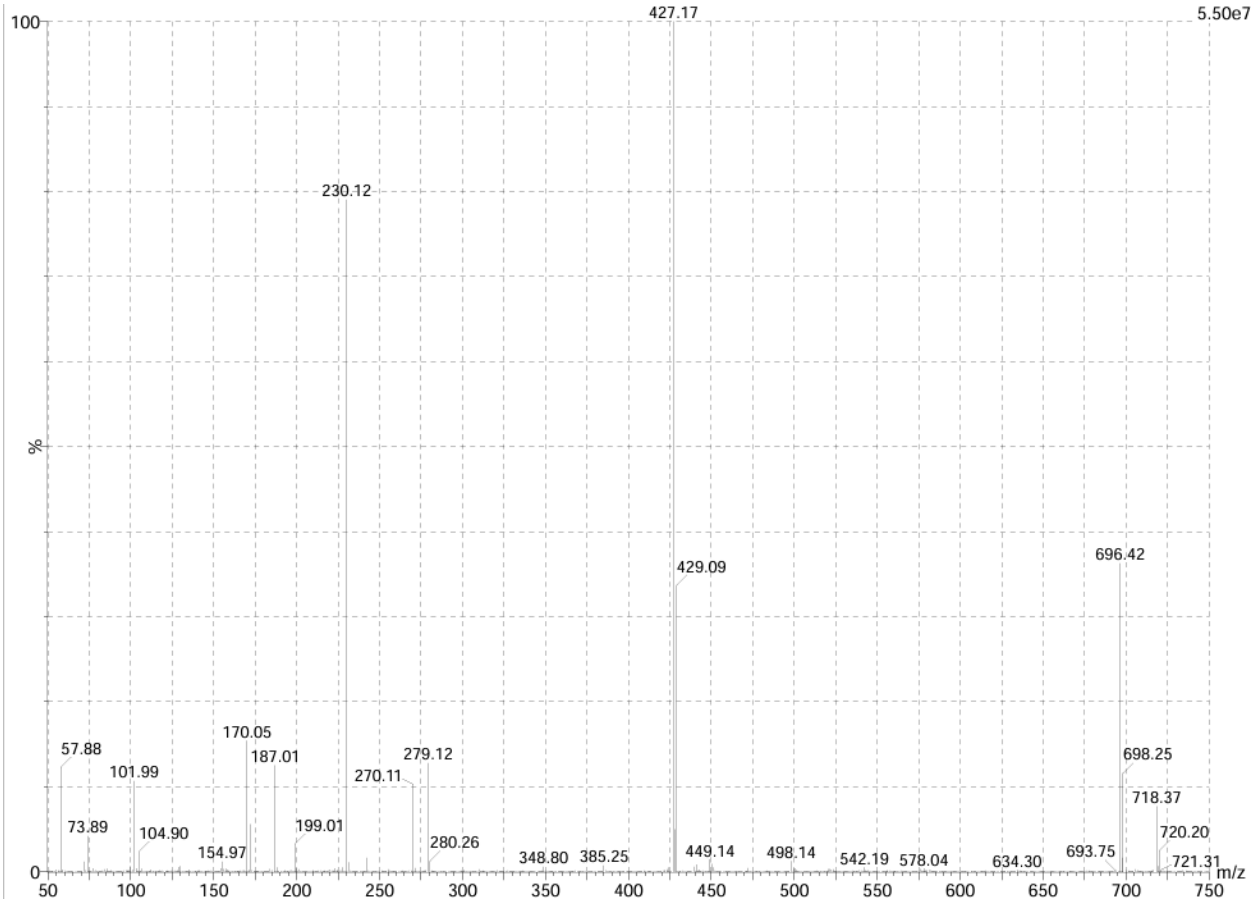

2-(benzyloxy)-5-chloroaniline

Diode Array (254 nm)

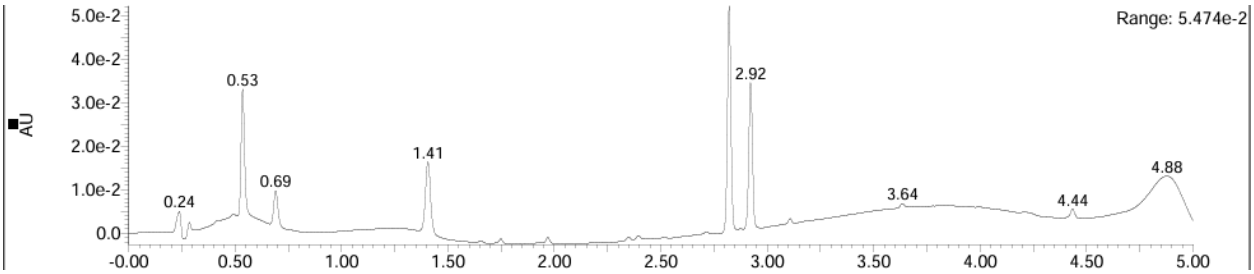

ESI+

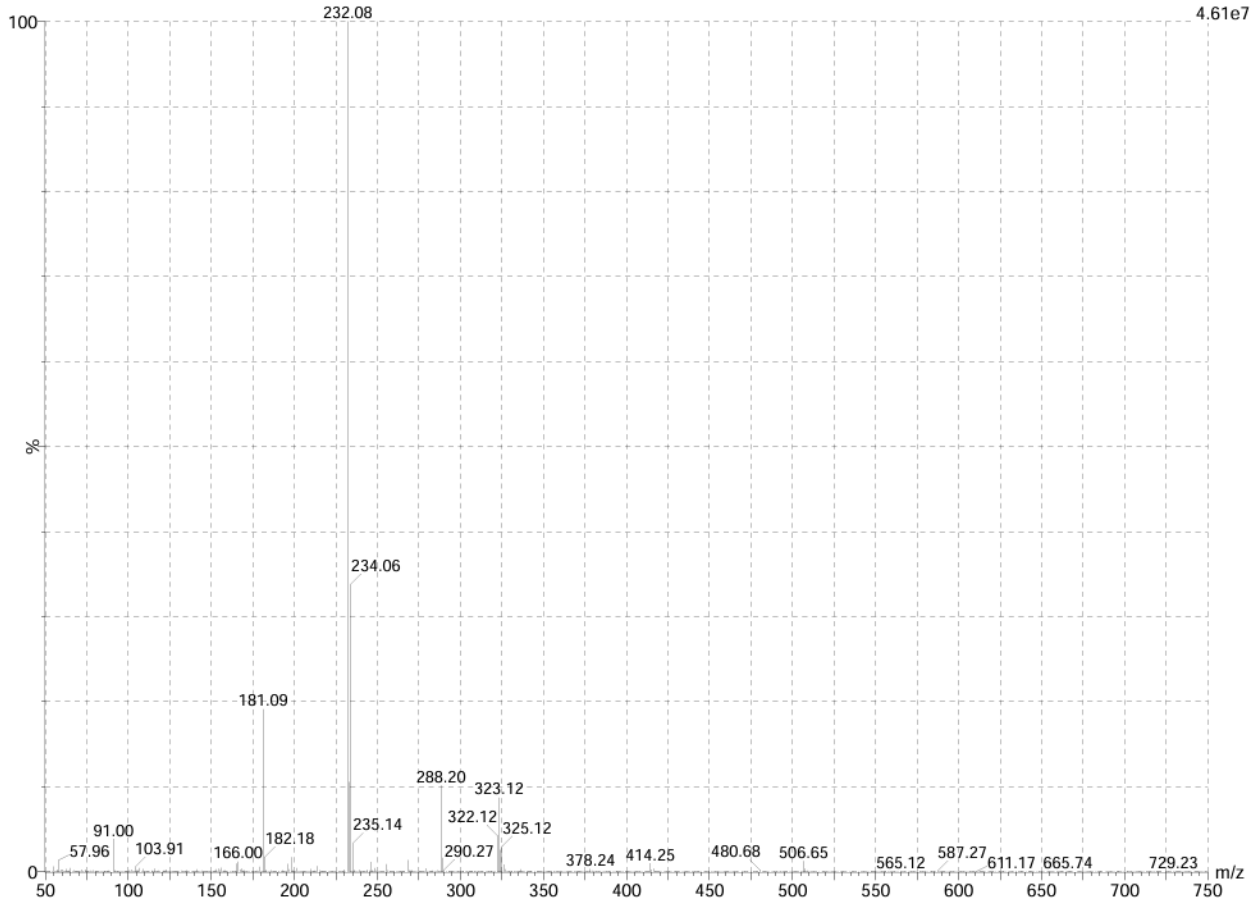

^{18}F-Fluorination Radio-TLC Data

Positive Control Reaction

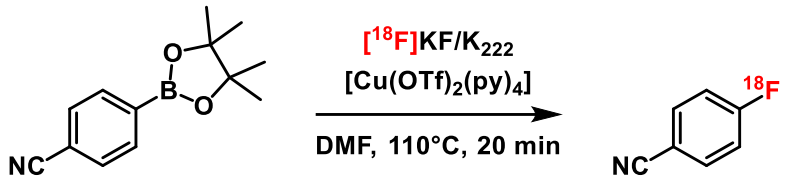

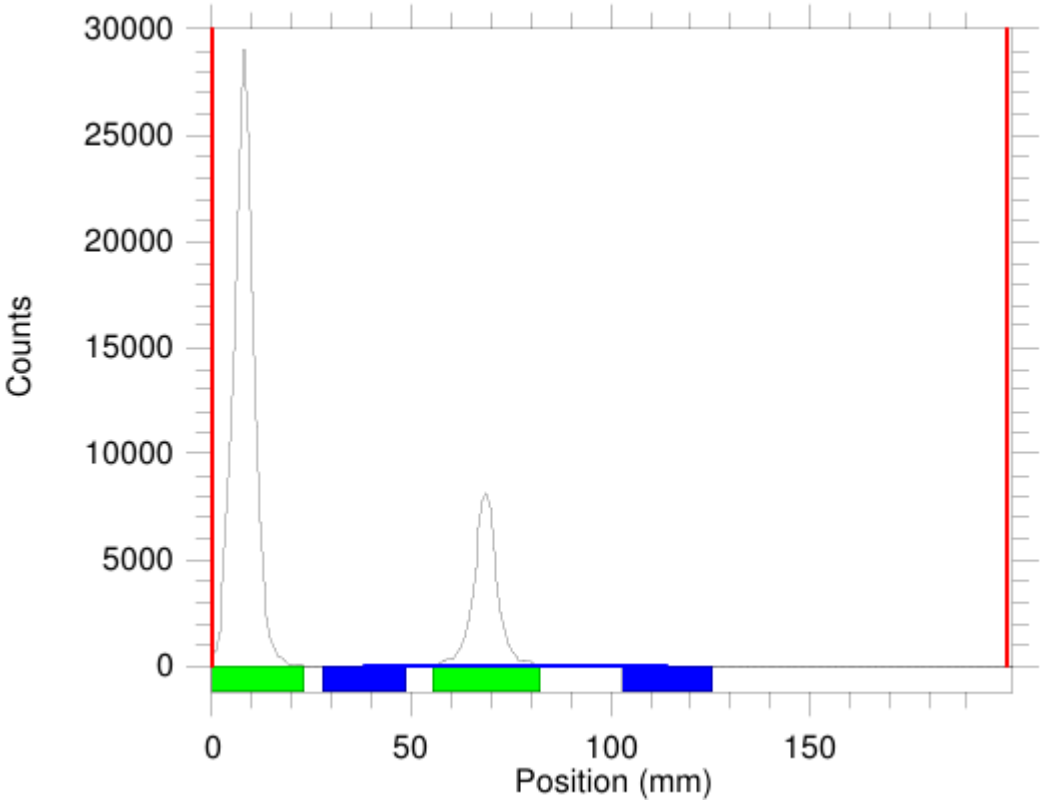

ASP4345 Screening Reaction